Contemporary Mathematics

Adaptive Finite Element Methods in Flow Computations

Rolf Rannacher

Abstract. This article surveys recent developments of theory-based methods for mesh adaptivity and error control in the numerical solution of flow problems. The emphasis is on viscous incompressible flows governed by the Navier-Stokes equations. But also inviscid transsonic flows and viscous low-Mach number flows including chemical reactions are considered. The Galerkin finite element method provides the basis for a common rigorous a posteriori error analysis. A large part of the existing work on a posteriori error analysis deals with error estimation in global norms such as the 'energy norm' involving usually unknown stability constants. However, in most CFD applications, the error in a global norm does not provide useful bounds for the errors in the quantities of real physical interest. Such 'goal-oriented' error bounds can be derived by duality arguments borrowed from optimal control theory. These a posteriori error estimates provide the basis of a feedback process for successively constructing economical meshes and corresponding error bounds tailored to the particular goal of the computation. This approach, called the 'dual-weighted-residual method' (DWR method), is developed within an abstract functional analytic setting, thus providing the general guideline for applications to various kinds of flow models including also aspects of flow control and hydrodynamic stability. Several examples are discussed in order to illustrate the main features of the DWR method.

Contents

1991 *Mathematics Subject Classification.* Primary 76-02, 76M10, 76D05, 76D55; Secondary 65M50, 65M60, 65N30, 65N50, 65N25.

Key words and phrases. CFD, finite elements, adaptivity, error control, DWR method, eigenvalue problem, hydrodynamic stability, flow control.

This work has been supported by the Deutsche Forschungsgemeinschaft (DFG), through the Sonderforschungsbereich 'Reaktive Strömungen, Diffusion und Transport' (SFB 359) at the University of Heidelberg.

1. Introduction

We begin with a brief discussion of the philosophy underlying the approaches to self-adaptivity which will be discussed in this article. Let the goal of a simulation be the accurate and efficient computation of the value of a functional $J(u)$, the 'target quantity', with accuracy TOL from the solution u of a continuous model by using a discrete model of dimension N:

$$\mathcal{A}(u) = F, \quad \mathcal{A}_h(u_h) = F_h.$$

The evaluation of the solution by the output functional $J(\cdot)$ represents what we exactly want to know of a solution. This may be for instance the stress or pressure near a critical point, certain local mean values of species concentrations, the drag and lift coefficient of a body in a viscous liquid, etc. Then, the goal of adaptivity is the 'optimal' use of computing resources to achieve either *minimal work for prescribed accuracy*, or *maximal accuracy for prescribed work*. These goals are approached by automatic mesh adaptation on the basis of local 'error indicators' taken from the computed solution u_h on the current mesh $\mathbb{T}_h = \{K\}$. Examples are:

- error indicators based on pure 'regularity' information,
$$\eta_K^{\rm reg} := h_K \|D_h^2 u_h\|_K,$$
where $D_h^2 u_h$ are certain second-order difference quotients,
- error indicators based on local gradient recovery such as the well-known 'Zienkiewicz-Zhu indicator' (see Ainsworth and Oden [1]),
$$\eta_K^{\rm ZZ} := \|M_h(\nabla u_h) - \nabla u_h\|_K,$$
where $M_h(\nabla u_h)$ is obtained by locally averaging function values of ∇u_h,
- error indicators based on 'residual' information,
$$\eta_K^{\rm res} := h_K \|R(u_h)\|_K,$$
where $R(u_h)_{|K}$ are certain 'residuals' of the computed solution.

According to the size of the indicators the current mesh may be locally refined or coarsened, or a full remeshing may be performed. Although remeshing is very popular in CFD applications since it allows to use commercial mesh generators and to maintain certain mesh qualities, it also has some disadvantages. The most severe one is that remeshing destroys the regular hierarchical structure of successively refined meshes which makes the use of efficient multilevel or multigrid solvers difficult. Therefore, all examples presented in this article employ hierarchical mesh adaptation.

The 'residual-based' error indicators largely exploit the structure of the underlying differential equations. This requires an appropriate discretization which inherits as much as possible of the structure and properties of the continuous model. Here, the method of choice is the *'continuous' Galerkin Finite Element Method (cG-FEM)* which is particularly suited for approximating models governed by viscous terms, such as the Navier-Stokes equations for moderate Reynolds numbers. For inviscid models or those with dominant transport, such as the Euler equations, the *'discontinuous' Galerkin Finite Element Method (dG-FEM)* shares most of the features of the traditional *Finite Volume Method (FVM)* but is potentially more flexible with respect to mesh geometry and order of approximation. Both methods

are based on variational formulations of the differential equations to be solved and allow for the rigorous derivation of a priori as well as a posteriori error estimates.

The traditional approach to adaptivity aims at estimating the error with respect to the generic 'energy norm' of the problem in terms of the computable 'residual' $R(u_h) = `F - \mathcal{A}(u_h)'$ which is well defined in the context of a Galerkin finite element method,

$$\|u - u_h\|_E \le c\Big(\sum_{K\in\mathbb{T}_h} h_K^2 \rho_K^2 \Big)^{1/2}, \tag{1.1}$$

where $\rho_K := \|R(u_h)\|_K$, and the sum extends over all cells of the computational mesh $\mathbb{T}_h$. For references see the survey articles by Ainsworth and Oden [1] and Verfürth [57]. This approach seems rather generic as it is directly based on the variational formulation of the problem and allows to exploit its inherent coercivity properties. However, in most applications the error in the energy norm does not provide a useful bound on the error in the quantities of real physical interest. A more versatile method for a posteriori error estimation with respect to relevant error measures such as point values, line averages, etc., is obtained by using duality arguments as common from the *a priori* error analysis of finite element methods. This approach has been systematically developed by Johnson and his co-workers [20,44], and was then extended by the author and his group to a practical feedback method for mesh optimization termed 'Dual-Weighted Residual Method' (DWR method), Becker and Rannacher [10–12]. A general introduction to the DWR method and a variety of applications in different fields can be found in the survey article Becker and Rannacher [12] and the book Bangerth and Rannacher [2]. Variants of this approach have also been developed in the groups of A. T. Patera [47, 48, 52], and J. T. Oden [49, 50].

The DWR method yields *weighted* a posteriori error bounds with respect to prescribed 'output functionals' $J(u)$ of the solution, of the form

$$|J(u) - J(u_h)| \le \sum_{K\in\mathbb{T}_h} h_K \rho_K \omega_K, \tag{1.2}$$

where the weights ω_K are obtained by approximately solving a linearized *dual problem*, $\mathcal{A}'(u)^* z = J(\cdot)$. The *dual solution* z may be viewed as a generalized Green function with respect to the output functional $J(\cdot)$, and accordingly the weight ω describes the effect of variations of the residual $\rho(u_h)$ on the error $J(u) - J(u_h)$ as consequence of mesh adaptation. This accomplishes control of

- error propagation in space (global pollution effect),
- interaction of various physical error sources (local sensitivity analysis).

In practice it is mostly impossible to determine the complex error interaction by analytical means, it rather has to be detected by computation. This automatically leads to a feed-back process in which error estimation and mesh adaptation go hand-in-hand leading to economical discretization for computing the quantities of interest. In this article, we concentrate the discussion of numerical methods for flow problems to the two extreme cases of (i) purely inviscid flow for positive Mach number (Euler equations) and (ii) diffusion dominated flow for zero or small Mach number (Navier-Stokes equations). Of course, in real-life applications both phenomena may occur simultaneously in different parts of the flow domain.

In Section 2, we develop the DWR method within an abstract functional analytic setting which afterwards allows for applications to the Galerkin approximation of variational equations and optimal control problems as well as stability eigenvalue problems. In Section 3, we discuss the practical realization of the DWR method for several model situations. Then in Section 4, we apply these techniques to various types of flow problems ranging from purely inviscid flow (Euler equations) over viscous incompressible (Navier-Stokes equations) to heat-driven flow with chemical reactions. Several examples are discussed in order to illustrate the main features of the DWR method. Most of these examples are collected from earlier articles Braack and Rannacher [16], Rannacher [53], and Becker and Rannacher [12], but also new, not yet published, material is included.

2. The Dual Weighted Residual (DWR) method

2.1. The abstract framework. The theoretical basis of the DWR method is laid within the abstract framework of Galerkin approximation of variational equations in Hilbert space. The following presentation is adopted from Becker and Rannacher [12].

2.2. Approximation of stationary points. Let X be a Hilbert space and $L(\cdot)$ a differentiable functional on X. Its first-, second-, and third-order derivatives at some $x \in X$ are denoted by $L'(x)(\cdot)$, $L''(x)(\cdot,\cdot)$, and $L'''(x)(\cdot,\cdot,\cdot)$, respectively. Suppose that $x \in X$ is a stationary point of $L(\cdot)$ satisfying

$$L'(x)(y) = 0 \quad \forall y \in X. \tag{2.1}$$

This equation is approximately solved by a Galerkin method using finite-dimensional subspaces $X_h \subset X$, parametrized by $h \in \mathbb{R}_+$. We seek $x_h \in X_h$ satisfying

$$L'(x_h)(y_h) = 0 \quad \forall\, y_h \in X_h. \tag{2.2}$$

For estimating the difference $L(x) - L(x_h)$, we start from the trivial identity

$$L(x) - L(x_h) = \int_0^1 L'(x_h + se)(e)\,\mathrm{d}s + \tfrac{1}{2}L'(x_h)(e_h) - \tfrac{1}{2}\big\{L'(x_h)(e) + L'(x)(e)\big\},$$

where $e := x - x_h$. Here, the last two terms in brackets on the right can be interpreted as the trapezoidal rule approximation of the integral term. Hence, recalling the corresponding error representation and using (2.2), we obtain the following result.

THEOREM 2.1. *For any solutions of the problems (2.1) and (2.2), we have the a posteriori error representation*

$$L(x) - L(x_h) = \tfrac{1}{2}L'(x_h)(x - y_h) + \mathcal{R}_h, \tag{2.3}$$

for arbitrary $y_h \in X_h$. The remainder term $\mathcal{R}_h$ is cubic in the error e,

$$\mathcal{R}_h := \tfrac{1}{2}\int_0^1 L'''(x_h + se)(e,e,e)\, s(s-1)\,\mathrm{d}s.$$

REMARK 2.2. In view of the possible nonuniqueness of the solutions x and x_h, the formulated goal of estimating the error quantity $L(x) - L(x_h)$ needs some explanation. The error representation (2.3) does not explicitly require that the approximation x_h is close to x. However, since it contains a remainder term in which the difference $x - x_h$ occurs, the result is useful only under the assumption that the convergence $x_h \to x$, as $h \to 0$, is known by *a priori* arguments.

2.3. Approximation of variational equations. Let $A(\cdot)(\cdot)$ be a differentiable semi-linear form and $F(\cdot)$ a linear functional defined on some Hilbert space V. We seek a solution $u \in V$ to the variational equation

$$A(u)(\varphi) = F(\varphi) \quad \forall\, \varphi \in V. \tag{2.4}$$

For a finite-dimensional subspace $V_h \subset V$, again parametrized by $h \in \mathbb{R}_+$, the corresponding Galerkin approximation $u_h \in V_h$ is determined by

$$A(u_h)(\varphi_h) = F(\varphi_h) \quad \forall\, \varphi_h \in V_h. \tag{2.5}$$

We assume that equations (2.4) and (2.5) possess solutions (not necessarily unique). Let the goal of the computation be the evaluation $J(u)$, where $J(\cdot)$ is a given differentiable functional. We want to embed this situation into the general setting of Theorem 2.1. To this end, we note that computing $J(u)$ from the solution of (2.4) can be interpreted as computing a stationary point $\{u, z\} \in V \times V$ of the Lagrangian

$$L(u, z) := J(u) - A(u)(z) + F(z),$$

with the dual variable $z \in V$, that is solving

$$A(u)(\psi) = F(\psi) \quad \forall \psi \in V, \tag{2.6}$$

$$A'(u)(\varphi, z) = J'(u)(\varphi) \quad \forall \varphi \in V. \tag{2.7}$$

In order to obtain a discretization of the system (2.6–2.7), in addition to (2.5), we solve the discrete adjoint equation

$$A'(u_h)(\varphi_h, z_h) = J'(u_h)(\varphi_h), \quad \varphi_h \in V_h. \tag{2.8}$$

We suppose that the dual problems also possess solutions $z \in V$ and $z_h \in V_h$, respectively. Notice that at the solutions $x = \{u, z\} \in X := V \times V$ and $x_h = \{u_h, z_h\} \in X_h := V_h \times V_h$, there holds

$$L(u, z) - L(u_h, z_h) = J(u) - J(u_h).$$

Hence, Theorem 2.1, applied to the Lagrangian $L(\cdot)(\cdot)$ on X yields a representation for the error $J(u) - J(u_h)$ in terms of the residuals

$$\rho(u_h)(\psi) := F(\psi) - A(u_h)(\psi),$$
$$\rho^*(z_h)(\varphi) := J'(u_h)(\varphi) - A'(u_h)(\varphi, z_h).$$

Since $L(u)(z)$ is linear in z, the remainder $\mathcal{R}_h$ only consists of the following three terms:

$$J'''(u_h + se)(e, e, e) - A'''(u_h + se)(e, e, e, z_h + se^*) - 3A''(u_h + se)(e, e, e^*).$$

This leads us to the following result.

THEOREM 2.3. *For any solutions of the Euler-Lagrange systems (2.6,2.7) and (2.5,2.8), we have the a posteriori error representation*

$$J(u) - J(u_h) = \tfrac{1}{2}\rho(u_h)(z - \psi_h) + \tfrac{1}{2}\rho^*(z_h)(u - \varphi_h) + \mathcal{R}_h, \tag{2.9}$$

for arbitrary ψ_h, $\varphi_h \in V_h$. The remainder term $\mathcal{R}_h$ is cubic in the errors $e := u - u_h$ and $e^* := z - z_h$,

$$\mathcal{R}_h := \tfrac{1}{2}\int_0^1 \big\{J'''(u_h + se)(e, e, e) - A'''(u_h + se)(e, e, e, z_h + se^*) - 3A''(u_h + se)(e, e, e^*)\big\}\, s(s-1)\,\mathrm{ds}.$$

The remainder term $\mathcal{R}_h$ in (2.9) is usually neglected. The evaluation of the resulting error estimator

$$\eta(u_h) := \tfrac{1}{2}\rho(u_h)(z-\psi_h) + \tfrac{1}{2}\rho^*(z_h)(u-\varphi_h),$$

for arbitrary $\psi, \varphi \in V$, requires us to determine approximations to the exact primal and dual solutions u and z, respectively.

REMARK 2.4. We note that the error representation (2.9) is the nonlinear analogue of the trivial identity

$$J(e) = \rho(u_h)(z-\psi_h) = \rho^*(z_h)(u-\varphi_h) = F(e^*), \tag{2.10}$$

in the linear case, for arbitrary $\varphi_h, \psi_h \in V_h$.

Integrating by parts in (2.9), we can derive a simpler error representation that does not contain the unknown primal solution u,

$$J(u) - J(u_h) = \rho(u_h)(z - \psi_h) + \tilde{\mathcal{R}}_h, \tag{2.11}$$

for arbitrary $\psi_h \in V_h$, with the remainder term

$$\tilde{\mathcal{R}}_h = \int_0^1 \big\{A''(u_h + se)(e,e,z) - J''(u_h + se)(e,e)\big\}s\,\mathrm{ds}.$$

The evaluation of (2.11) only requires a guess for the dual solution z, but the remainder term $\tilde{\mathcal{R}}_h$ is only quadratic in the error e.

2.4. Approximation of optimization problems. We continue using the notation from above. A differentiable 'cost-functional' $J(u,q)$ is now to be minimized under the equation constraint (2.4),

$$J(u,q) \;\to\; \min, \qquad A(u,q)(\varphi) = F(\varphi) \quad \forall \varphi \in V, \tag{2.12}$$

where q is the control from the 'control space' Q, and $A(\cdot,\cdot)(\cdot)$ is a differentiable semi-linear form on $V \times Q \times V$. On the space $X := V \times Q \times V$, we introduce the Lagrangian

$$L(u,q,\lambda) \;:=\; J(u,q) - A(u,q)(\lambda) + F(\lambda),$$

with the adjoint variable $\lambda \in V$. We want to compute stationary points $x = \{u,q,\lambda\} \in X$ of L, that is solutions of the variational equation

$$L'(x)(y) = 0 \quad \forall y \in X. \tag{2.13}$$

This is equivalent to the saddle-point system

$$A'_u(u,q)(\varphi,\lambda) \;=\; J'_u(u,q)(\varphi) \quad \forall \varphi \in V, \tag{2.14}$$

$$A(u,q)(\psi) \;=\; F(\psi) \quad \forall \psi \in V, \tag{2.15}$$

$$A'_q(u,q)(\chi,\lambda) \;=\; J'_q(u,q)(\chi) \quad \forall \chi \in Q. \tag{2.16}$$

For discretization of equation (2.13), we introduce finite dimensional subspace $V_h \subset V$ and $Q_h \subset Q$ parametrized by $h \in \mathbb{R}_+$, and set $X_h := V_h \times Q_h \times V_h \subset X$. Then, approximations $x_h = \{u_h, q_h, \lambda_h\} \in X_h$ are determined by

$$L'(x_h)(y_h) = 0 \quad \forall y_h \in X_h, \tag{2.17}$$

what is equivalent to the discrete saddle-point problem

$$A'_u(u_h,q_h)(\varphi_h,\lambda_h) \;=\; J'_u(u_h,q_h)(\varphi_h) \quad \forall \varphi_h \in V, \tag{2.18}$$

$$A(u_h,q_h)(\psi_h) \;=\; F(\psi_h) \quad \forall \psi_h \in V_h, \tag{2.19}$$

$$A'_q(u_h,q_h)(\chi_h,\lambda_h) \;=\; J'_q(u_h,q_h)(\chi_h) \quad \forall \chi_h \in Q_h. \tag{2.20}$$

The residuals of these equations are defined by

$$\begin{aligned}
\rho^*(\lambda_h)(\cdot) &:= J'_u(u_h,q_h)(\varphi_h) - A'_u(u_h,q_h)(\varphi_h,\lambda_h),\\
\rho(u_h)(\cdot) &:= F(\psi_h) - A(u_h,q_h)(\psi_h),\\
\rho^{**}(q_h)(\cdot) &:= J'_q(u_h,q_h)(\chi_h) - A'_q(u_h,q_h)(\chi_h,\lambda_h).
\end{aligned}$$

Again, since the pairs $\{u,q\}$ and $\{u_h,q_h\}$ satisfy the state equations, we have

$$L(u,q,\lambda) - L(u_h,q_h,\lambda_h) = J(u) - J(u_h).$$

Then, as before, we obtain from Theorem 2.1 the following result.

THEOREM 2.5. *For any solutions of the saddle point problems (2.14- 2.16) and (2.18-2.20), we have the a posteriori error representation*

$$\begin{aligned}
J(u) - J(u_h) = \tfrac{1}{2}\rho(u_h)(\lambda-\psi_h) + \tfrac{1}{2}\rho^*(\lambda_h)(u-\varphi_h)\\
+ \tfrac{1}{2}\rho^{**}(q_h)(q-\chi_h) + \mathcal{R}_h,
\end{aligned} \tag{2.21}$$

for arbitrary φ_h, $\psi_h \in V_h$ *and* $\chi_h \in Q_h$. *The remainder term* $\mathcal{R}_h$ *is cubic in the errors* $e^u := u - u_h$, $e^\lambda := \lambda - \lambda_h$ *and* $e^q := q - q_h$.

2.5. Approximation of stability eigenvalue problems. Let $\hat{u}$ and $\hat{u}_h$ be a base solution and its approximation given by the equations (2.4) and (2.5), respectively. We consider the eigenvalue problem associated with the linearization of the semi-linear form $a(\cdot)(\cdot)$ about $\hat{u}$,

$$a'(\hat{u})(u,\varphi) = \lambda\, m(u,\varphi) \quad \forall \varphi \in V, \tag{2.22}$$

and its discrete analogues,

$$a'(\hat{u}_h)(u_h,\varphi_h) = \lambda_h\, m(u_h,\varphi_h) \quad \forall \varphi_h \in V_h. \tag{2.23}$$

Here, $m(\cdot,\cdot)$ is a symmetric, semi-definite bilinear form on V. We assume that $a'(\hat{u}_h)(\cdot,\cdot)$ is coercive on V and that $m(\cdot,\cdot)$ is compact, such that the Fredholm theory applies to this eigenvalue problem. From the eigenvalues $\lambda \in \mathbb{C}$ of (2.22) one can obtain information about the (dynamic) stability of the base solution $\hat{u}$. For $\mathrm{Re}\lambda > 0$ it is said to be 'linearly stable' and for $\mathrm{Re}\lambda < 0$ 'linearly unstable'. The related aspects of 'linear (hydrodynamic) stability theory' will be discussed in more detail below.

In order to derive an *a posteriori* estimate for the eigenvalue error $\lambda - \lambda_h$, we introduce the spaces $\mathcal{V} := V \times V \times \mathbb{C}$ and $\mathcal{V}_h := V_h \times V_h \times \mathbb{C}$, and denote their elements by $U := \{\hat{u}, u, \lambda\}$ and $U_h := \{\hat{u}_h, u_h, \lambda_h\}$, respectively. Further, for $\Phi = \{\hat{\varphi}, \varphi, \mu\} \in \mathcal{V}$, we introduce a semi-linear form $A(\cdot)(\cdot)$ by

$$A(U)(\Phi) := f(\hat{\varphi}) - a(\hat{u})(\hat{\varphi}) - a'(\hat{u})(u,\varphi) + \lambda\, m(u,\varphi) + \overline{\mu}\big\{m(u,u) - 1\big\}.$$

With this notation equations (2.4,2.22) and (2.5,2.23) in compact form read:

$$A(U)(\Phi) = 0 \quad \forall \Phi \in \mathcal{V}, \tag{2.24}$$

$$A(U_h)(\Phi_h) = 0 \quad \forall \Phi_h \in \mathcal{V}_h. \tag{2.25}$$

For controlling the error of this approximation, we choose the functional

$$J(\Phi) := \mu\, m(\varphi,\varphi),$$

for $\Phi = \{\hat\varphi, \varphi, \mu\} \in \mathcal{V}$, what is motivated by the fact that $J(U) = \lambda$, since $m(u,u) = 1$. In order to apply the general result of Theorem 2.3 to this situation, we have to identify the dual problems corresponding to (2.24) and (2.25). The dual solutions $Z = \{\hat z, z, \pi\} \in \mathcal{V}$ and $Z_h = \{\hat z_h, z_h, \pi_h\} \in \mathcal{V}_h$ are determined by the equation

$$A'(U)(\Phi, Z) = J'(U)(\Phi) \quad \forall \Phi \in \mathcal{V}, \tag{2.26}$$

and its discrete analogue

$$A'(U_h)(\Phi_h, Z_h) = J'(U_h)(\Phi_h) \quad \forall \Phi_h \in \mathcal{V}_h, \tag{2.27}$$

respectively. By a straightforward calculation (for the details see Heuveline and Rannacher [36]), we find that the dual solution $Z = \{\hat z, z, \pi\} \in \mathcal{V}$ is given by $z = u^*$ and $\pi = \lambda$, while $\hat z = \hat u^*$ is determined as solution of

$$a'(\hat u)(\psi, \hat u^*) = -a''(\hat u)(\psi, u, u^*) \quad \forall \psi \in V. \tag{2.28}$$

The corresponding residuals are defined by

$$\begin{aligned}
\rho(\hat u_h)(\psi) &:= f(\psi) - a(\hat u_h;\psi)\\
\rho^*(\hat u_h^*)(\psi) &:= -a''(\hat u)(\psi, u_h, u_h^*) - a'(\hat u_h)(\psi, \hat u_h^*),\\
\rho(u_h,\lambda_h)(\psi) &:= \lambda_h\, m(u_h,\psi) - a'(\hat u_h)(u_h,\psi),\\
\rho^*(u_h^*,\lambda_h)(\psi) &:= \lambda_h\, m(\psi,u_h^*) - a'(\hat u_h)(\psi,u_h^*).
\end{aligned}$$

Then, from Theorem 2.3, we obtain the following result.

THEOREM 2.6. *For the eigenvalue approximation, we have the error representation*

$$\begin{aligned}
\lambda - \lambda_h = {}& \tfrac12\big\{\rho(\hat u_h)(\hat u^* - \hat\psi_h) + \rho^*(\hat u_h^*;\hat u - \hat\varphi_h)\big\}\\
&+ \tfrac12\big\{\rho(u_h,\lambda_h)(u^* - \psi_h) + \rho^*(u_h^*,\lambda_h)(u - \varphi_h)\big\} - \mathcal{R}_h,
\end{aligned} \tag{2.29}$$

with arbitrary $\hat\psi_h$, ψ_h, $\hat\varphi_h$, $\varphi_h \in V_h$. The cubic remainder $\mathcal{R}_h$ is given by

$$\mathcal{R}_h = \tfrac12(\lambda - \lambda_h)(e^v, e^{v*}) - \tfrac{1}{12}a''(\hat u)(\hat e, \hat e, \hat e^*) - \tfrac{1}{12}a''(\hat u)(\hat e, e, e^*),$$

where $\hat e^v := \hat v - \hat v_h$, $\hat e^{v*} := \hat v^* - \hat v_h^*$, $e^v := v - v_h$, and $e^{v*} := v^* - v_h^*$.

REMARK 2.7. The result of Theorem 2.5 does not require the eigenvalue λ to be simple or non-degenerate. However, this is the generic case in most practical applications. The test for $m(v_h^*, v_h^*) \to \infty$ or $m(v_h^*, v_h^*) \gg 1$ can be used to detect either the degeneracy of the eigenvalue λ or, in the case $0 < \mathrm{Re}\lambda \ll 1$, the extension of the corresponding 'pseudo-spectrum' into the negative complex half-plane which indicates possible dynamic instability of the base flow. For a more detailed discussion of this point, we refer to Heuveline and Rannacher [36].

3. Model problems and practical aspects

In this section, we describe the application of the foregoing abstract theory to prototypical model situations which usually occur as components of flow models. In this context, we also discuss the practical evaluation of the a posteriori error representations and their use for automatic mesh adaptation. The first model case is the *elliptic* Poisson equation, the second one a purely *hyperbolic* transport problem, and the third one the *parabolic* heat equation.

3.1. Elliptic model case: Poisson equation. At first, we consider the model problem

$$-\Delta u = f \quad \text{in } \Omega, \quad u = 0 \ \text{ on } \partial\Omega, \tag{3.1}$$

on a polygonal domain $\Omega \subset \mathbb{R}^2$. Below, we will need some notation from the theory of functions spaces which is provided in the following subsection. Readers who are familiar with the usual Lebesgue- and Sobolev-space notation may want to skip this and continue with the next subsection on finite element approximation.

3.1.1. *Function spaces notation.* For an open set $G \subset \mathbb{R}^d$, we denote by $L^2(G)$ the Lebesgue space of square-integrable functions defined on G which is a Hilbert space provided with the scalar product and norm

$$(v,w)_G = \int_G vw\,dx, \quad \|v\|_G = \Big(\int_G |v|^2\,dx\Big)^{1/2}.$$

Analogously, $L^2(\partial G)$ denotes the space of square-integrable functions defined on the boundary ∂G equipped with the inner product and norm $(v,w)_{\partial G}$ and $\|v\|_{\partial G}$. The Sobolev spaces $H^1(G)$ and $H^2(G)$ consist of those functions $v \in L^2(G)$ which possess first- and second-order (distributional) derivatives $\nabla v \in L^2(G)^d$ and $\nabla^2 v \in L^2(G)^{d\times d}$, respectively. For functions in these spaces, we use the semi-norms

$$\|\nabla v\|_G = \Big(\int_G |\nabla v|^2\,dx\Big)^{1/2}, \quad \|\nabla^2 v\|_G = \Big(\int_G |\nabla^2 v|^2\,dx\Big)^{1/2}.$$

The space $H^1(G)$ is continuously embedded in the space $L^2(\partial G)$, such that for each $v \in H^1(G)$ there exists a *trace* $v_{|\partial G} \in L^2(\partial G)$. In this notation, we do not distinguish between the function v on G and its trace on ∂G. Further, the functions in the subspace $H^1_0(G) \subset H^1(G)$ are characterized by the property $v_{|\partial G} = 0$. By the Poincaré inequality, $\|v\|_G \le c\|\nabla v\|_G$ for $v \in H^1_0(G)$, the H^1-semi-norm $\|\nabla v\|_G$ is a norm on the subspace $H^1_0(G)$. If the set G is the set Ω on which the differential equation is posed, we usually omit the subscript Ω in the notation of norms and scalar products, e.g., $(v,w) = (v,w)_\Omega$ and $\|v\| = \|v\|_\Omega$.

3.1.2. *Variational formulation and finite element approximation.* The natural solution space for the boundary value problem (3.1) is the Sobolev space $V = H^1_0(\Omega)$ defined above. The variational formulation of (3.1) seeks $u \in V$, such that

$$(\nabla u, \nabla\varphi) = (f,\varphi) \quad \forall \varphi \in V. \tag{3.2}$$

The finite element approximation of (3.2) uses finite dimensional subspaces

$$V_h = \{v \in V : v_{|K} \in P(K),\ K \in \mathbb{T}_h\},$$

defined on decompositions $\mathbb{T}_h$ of Ω into triangles or quadrilaterals K (*cells*) of width $h_K = diam(K)$; we write $h = \max_{K\in\mathbb{T}_h} h_K$ for the *global* mesh width. Here, $P(K)$ denotes a suitable space of polynomial-like functions defined on the

cell $K \in \mathbb{T}_h$. We will mainly consider low-order finite elements on quadrilateral meshes where $P(K) = \tilde{Q}_1(K)$ consists of shape functions which are obtained as usual via a bilinear transformation from the space of bilinear functions $Q_1(\hat{K}) = \text{span}\{1, x_1, x_2, x_1x_2\}$ on the reference cell $\hat{K} = [0,1]^2$ (*isoparametric bilinears*). Local mesh refinement or coarsening is realized by using *hanging nodes*. The variable corresponding to such a hanging node is eliminated from the system by linear interpolation of neighboring variables in order to preserve the conformity of the global ansatz, i.e., $V_h \subset V$ (for more details we refer to Carey and Oden [19]). The discretization of (3.2) determines $u_h \in V_h$ by

$$(\nabla u_h, \nabla\varphi_h) = (f, \varphi_h) \quad \forall\varphi_h \in V_h. \tag{3.3}$$

The essential feature of this approximation scheme is the *Galerkin orthogonality* of the error $e = u - u_h$,

$$(\nabla e, \nabla\varphi_h) = 0, \quad \varphi_h \in V_h. \tag{3.4}$$

3.1.3. *A priori error analysis.* We begin with a brief discussion of the a priori error analysis for the scheme (3.3). By $i_h u \in V_h$, we denote the natural nodal interpolant of $u \in C(\bar{\Omega})$ satisfying $i_h u(P) = u(P)$ at all nodal points P. There holds (see, e.g., Brenner and Scott [18]):

$$\|u - i_h u\|_K + h_K^{1/2}\|u - i_h u\|_{\partial K} + h_K\|\nabla(u - i_h u)\|_K \le c_i h_K^2 \|\nabla^2 u\|_K, \tag{3.5}$$

with some *interpolation constant* $c_i > 0$ independent of h_K and u. By the projection property of the Galerkin finite element scheme the interpolation estimate (3.5) directly implies the a priori *energy-norm* error estimate

$$\|\nabla e\| = \inf_{\varphi_h \in V_h} \|\nabla(u - \varphi_h)\| \le c_i h^2 \|\nabla^2 u\|. \tag{3.6}$$

Further, employing a duality argument (so-called *Aubin-Nitsche trick*),

$$-\Delta z = \|e\|^{-1} e \quad \text{in } \Omega, \quad z = 0 \ \text{ on } \partial\Omega, \tag{3.7}$$

we obtain

$$\|e\| = (e, -\Delta z) = (\nabla e, \nabla z) = (\nabla e, \nabla(z - i_h z) \le c_i c_s h \|\nabla e\|, \tag{3.8}$$

where the *stability constant* c_s is defined by the a priori bound $\|\nabla^2 z\| \le c_s$. Together with the energy-error estimate (3.6), this implies the improved a priori L^2-norm error estimate

$$\|e\| \le c_i^2 c_s h^2 \|\nabla^2 u\| \le c_i^2 c_s^2 h^2 \|f\|. \tag{3.9}$$

3.1.4. *A posteriori error analysis.* Next, we seek to derive a posteriori error estimates. Let $J(\cdot)$ be an arbitrary (linear) *error functional* defined on V, and $z \in V$ the solution of the corresponding dual problem

$$(\nabla\varphi, \nabla z) = J(\varphi) \quad \forall\varphi \in V. \tag{3.10}$$

Taking $\varphi = e$ in (3.10) and using the Galerkin orthogonality (3.4), in accordance with the general result of Theorem 2.3 and the relation (2.10), we obtain after cell-wise integration by parts the error representation

$$\begin{aligned} J(e) &= \rho(u_h)(z - \varphi_h) = (\nabla e, \nabla(z - \varphi_h)) \\ &= \sum_{K \in \mathbb{T}_h} \big\{(-\Delta u + \Delta u_h, z - \varphi_h)_K - (\partial_n u_h, z - \varphi_h)_{\partial K}\big\}. \end{aligned}$$

This can be rewritten as

$$J(e) = \eta(u_h) := \sum_{K\in\mathbb{T}_h} \big\{(R_h, z-\varphi_h)_K + (r_h, z-\varphi_h)_{\partial K}\big\}, \tag{3.11}$$

with an arbitrary $\varphi_h \in V_h$, and 'cell-' and 'edge-residuals' defined by

$$R_{h|K} = f + \Delta u_h, \qquad r_{h|\Gamma} := \begin{cases} -\frac{1}{2}[\partial_n u_h], & \text{if } \Gamma \subset \partial K \setminus \partial\Omega, \\ -\partial_n u_h, & \text{if } \Gamma \subset \partial\Omega, \end{cases}$$

where $[\nabla u_h]$ denotes the jump of ∇u_h across the cell edges Γ. From the error identity (3.11), we can infer an a posteriori error estimate of the form

$$|J(e)| \le |\eta(u_h)| = \sum_{K\in\mathbb{T}_h} |\eta_K(u_h)|, \tag{3.12}$$

with the cell-wise error indicators

$$\eta_K(u_h) := (R_h, z-\varphi_h)_K + (r_h, z-\varphi_h)_{\partial K}.$$

These indicators are 'consistent' in the sense that they vanish at the exact solution, $\eta_K(u) = 0$.

THEOREM 3.1. *For the finite element approximation of the Poisson equation (3.1), there holds the a posteriori error estimate with respect to a functional $J(\cdot)$:*

$$|J(e_h)| \le \sum_{K\in\mathbb{T}_h} \rho_K\, \omega_K, \tag{3.13}$$

with the cell residuals ρ_K and weights ω_K defined by

$$\rho_K := \big(\|R_h\|_K^2 + h_K^{-1}\|r_h\|_{\partial K}^2\big)^{1/2}, \quad \omega_K := \big(\|z - i_h z\|_K^2 + h_K\|z - i_h z\|_{\partial K}^2\big)^{1/2}.$$

REMARK 3.2. In general, the transition from the error identity (3.11) to the error estimate (3.13) causes significant over-estimation of the true error. The weights ω_K describe the dependence of the error $J(e_h)$ on variations of the cell residuals ρ_K. In practice they have to be determined computationally.

REMARK 3.3. Since the relation (3.11) is an identity, any reformulation of it can be used for deriving estimates for the error $J(e)$. However, one has to be careful in extracting local refinement indicators. For example, one may prefer the form

$$J(e) = \sum_{K\in\mathbb{T}_h} \big\{(f, z-\varphi_h)_K - (\nabla u_h, \nabla(z-\varphi_h))_K\big\},$$

which does not require the evaluation of normal derivatives across the interelement boundaries. But the corresponding local error indicators

$$\eta_K(u_h) := (f, z-\varphi_h)_K - (\nabla u_h, \nabla(z-\varphi_h))_K$$

are not consistent, i.e., $\eta_K(u) \neq 0$. Mesh adaptation based on these inconsistent error indicators generally results in unnecessary over-refinement.

REMARK 3.4. Another approach to goal-oriented a posteriori error estimation uses so-called 'gradient recovery techniques' in the spirit of the ZZ approach. ¿From the dual equation (3.10) employing Galerkin orthogonality, we obtain the error identity

$$J(e) = (\nabla e, \nabla e^*), \tag{3.14}$$

with the primal and dual errors $e = u - u_h$ and $e^* = z - z_h$, respectively. Let $M_K(\nabla u_h)$ be an approximation obtained by local averaging, satisfying

$$\|\nabla u - M_K(\nabla u_h)\|_K \ll \|\nabla u - \nabla u_h\|_K.$$

Then,

$$J(e) \approx \sum_{K\in\mathbb{T}_h} (M_K(\nabla u_h) - \nabla u_h, M_K(\nabla z) - \nabla z_h)_K,$$

and the mesh adaptation may be based on the local error indicators

$$\eta_K(u_h) := (M_K(\nabla u_h) - \nabla u_h, M_K(\nabla z) - \nabla z_h)_K.$$

For more details on this method see Korotov, Neitaanmäki and Repin [46]. Its possible success depends on the reliability of the approximation $M_K(\nabla u_h) \approx \nabla u$ which is to be expected only for isotropic elliptic problems.

Remark 3.5. The error representation (3.11) seems to suggest that the use of differently refined meshes for u and z may be advisable according to their mutual singularities. However, this is a misconception as it does not observe the special role of the *multiplicative* interaction between primal residuals and dual weights. *Primal and dual solutions do not need to be computed on different meshes if their singularities are located at different places.* This rule is confirmed even for hyperbolic problems.

3.1.5. *A posteriori energy-norm error bound.* By the same type of argument as used above, we can also derive the traditional global energy-norm error estimates. To this end, we choose the functional

$$J(\varphi) := \|\nabla e\|^{-1}(\nabla e, \nabla\varphi)$$

in the dual problem (3.10). Its solution $z \in V$ satisfies $\|\nabla z\| \le 1$. Applying Theorem 3.1, we obtain the estimate

$$\|\nabla e\| \le \sum_{K\in\mathbb{T}_h} \rho_K\,\omega_K \le \Big(\sum_{K\in\mathbb{T}_h} h_K^2\rho_K^2\Big)^{1/2}\Big(\sum_{K\in\mathbb{T}_h} h_K^{-2}\omega_K^2\Big)^{1/2},$$

with residual terms and weights as defined above. Now, we use the approximation estimate

$$\Big(\sum_{K\in\mathbb{T}_h}\Big\{h_K^{-2}\|z-\tilde{i}_h z\|_K^2 + h_K^{-1}\|z-\tilde{i}_h z\|_{\partial K}^2\Big\}\Big)^{1/2} \le \tilde{c}_i\,\|\nabla z\|, \tag{3.15}$$

where $\tilde{i}_h z \in V_h$ is a modified nodal interpolation which is defined and stable on $H^1(\Omega)$ (for the construction of such an operator see Brenner and Scott [18]). Using this, we easily deduce the a posteriori *energy-norm* error estimate

$$\|\nabla e\| \le \eta_E(u_h) = \tilde{c}_i\Big(\sum_{K\in\mathbb{T}_h} h_K^2\rho_K^2\Big)^{1/2}. \tag{3.16}$$

An analogous argument also yields the usual a posteriori L^2-norm error bound

$$\|e\| \le \eta_{L^2}(u_h) = c_i c_s\Big(\sum_{K\in\mathbb{T}_h} h_K^4\rho_K^2\Big)^{1/2}. \tag{3.17}$$

3.2. Evaluation of error estimates. ¿From the a posteriori error estimate (3.12), we want to deduce criteria for local mesh adaptation and for the final stopping of the adaptation process. To this end, we have to evaluate the local cell error indicators

$$\eta_K(u_h) := (R_h, z - \varphi_h)_K + (r_h, z - \varphi_h)_{\partial K},$$

for arbitrary $\varphi_h \in V_h$, and the global error estimator

$$\eta(u_h) = \sum_{K \in \mathbb{T}_h} \eta_K(u_h).$$

This requires the construction of an approximation $\tilde{z} \approx z \in V$, such that $\tilde{z} - i_h\tilde{z}$ can substitute $z - i_h z$, resulting in approximate cell error indicators

$$\tilde{\eta}_K(u_h) := (R_h, \tilde{z} - i_h\tilde{z})_K + (r_h, \tilde{z} - i_h\tilde{z})_{\partial K}$$

and the corresponding approximate error estimator

$$J(e) \approx \tilde{\eta}(u_h) := \sum_{K \in \mathbb{T}_h} \tilde{\eta}_K(u_h).$$

The goal is to achieve an optimal *effectivity index* for the error estimator $\tilde{\eta}(u_h)$,

$$I_{\text{eff}} := \lim_{TOL \to 0} \Big| \frac{\tilde{\eta}(u_h)}{J(e)} \Big| = 1\,.$$

Computational experience shows that asymptotic sharpness does not seem to be achievable with acceptable effort (see Becker and Rannacher [11]). With all the cheaper methods considered the effectivity index I_{eff} never really tends to one, but in most relevant cases stays well below two, what may actually be considered as good enough. There are two separate aspects to be considered: the sharpness of the global error bound $\tilde{\eta}(u_h)$ and the effectivity of the local error indicators $\tilde{\eta}_K$ which are used in the mesh refinement process.

Accurate a posteriori error estimation is a delicate matter. Already by once applying the triangle inequality,

$$|J(e)| = |\eta(u_h)| \le \sum_{K \in \mathbb{T}_h} |\eta_K(u_h)|, \tag{3.18}$$

asymptotic sharpness may be lost. This is seen, for instance, in the case $J(u) = u(0)$ when the exact as well as the approximate solution are anti-symmetric with respect to the x-axis meaning that $e(0) = 0$, but $\eta(u_h) \neq 0$.

Most practical ways of generating approximation $\tilde{z}$ are based on solving the dual problem numerically. Let $z_h \in V_h$ denote the approximation to z obtained on the current mesh by the same finite element ansatz as used for computing u_h.

1. Approximation by higher order methods: The dual problem is solved by using *biquadratic* finite elements on the current mesh yielding an approximation $z_h^{(2)}$ to z. The resulting error estimator is denoted by

$$\eta^{(1)}(u_h) := \sum_{K \in \mathbb{T}_h} \big\{ (R_h, z_h^{(2)} - i_h z_h^{(2)})_K + (r_h, z_h^{(2)} - i_h z_h^{(2)})_{\partial K} \big\}.$$

It is seen by theoretical analysis as well as by numerical experiments that $\eta^{(1)}(u_h)$ has optimal effectivity, $I_{\text{eff}} = 1$. This rather expensive way of evaluating the error estimator is useful only in certain circumstances, e.g., for very irregular dual problems such as occurring in the solution of the Euler equations.

2. Approximation by higher order interpolation: A cheaper strategy uses patchwise *biquadratic* interpolation of the bilinear approximation z_h on the current mesh yielding an approximation $i_{2h}^{(2)} z_h$ to z. This construction requires some special care for elements with hanging nodes, in order to preserve the higher order accuracy of the interpolation process. The resulting global error estimator is denoted by

$$\eta^{(2)}(u_h) := \sum_{K\in\mathbb{T}_h} \big\{(R_h, i_{2h}^{(2)} z_h - z_h)_K + (r_h, i_{2h}^{(2)} z_h - z_h)_{\partial K}\big\}.$$

This rather simple strategy turns out to be surprisingly effective in many different situations. It is actually used in most of the computational examples discussed below. For the Poisson text problem there holds $I_{\text{eff}} \approx 1-2$. For more details and for other strategies for evaluating the error estimators we refer to Becker and Rannacher [11, 12].

REMARK 3.6. If on the basis of a numerical approximation to the dual solution z an approximate error representation $\tilde\eta(u_h)$ has been generated, one may hope to obtain an improved approximation to the target quantity by setting

$$\tilde J(u_h) := J(u_h) + \tilde\eta(u_h) \approx J(u).$$

Such a 'post-processing' can significantly improve the accuracy in computing $J(u)$. This idea has been pursued in Giles and Pierce [25] and Giles and Süli [26], particularly for finite volume approximations of flow problems.

3.3. Strategies for mesh adaptation. We want to discuss some strategies for organizing local mesh adaptation on the basis of a posteriori error estimates as derived in the preceding section. Suppose that we have an a posteriori error estimate of the form

$$|J(u) - J(u_h)| \approx |\tilde\eta(u_h)| \le \sum_{K\in\mathbb{T}_h} |\tilde\eta_K|, \tag{3.19}$$

with local *cell-error indicators* $\tilde\eta_K = \tilde\eta_K(u_h)$. The prescribed error tolerance is TOL and the maximum number of mesh cells N_{max}.

(i) Error balancing strategy: Cycle through the mesh and seek to equilibrate the local error indicators according to

$$\tilde\eta_K \approx \frac{TOL}{N}, \quad N = \#\{K\in\mathbb{T}_h\}. \tag{3.20}$$

This process requires iteration with respect to the number of mesh cells N and eventually leads to $\tilde\eta(u_h) \approx TOL$.

(ii) Fixed fraction strategy: Order cells according to the size of $\tilde\eta_K$,

$$\tilde\eta_{K_N} \ge \cdots \ge \tilde\eta_{K_i} \cdots \ge \tilde\eta_{K_1},$$

and refine 20% of cells with largest $\tilde\eta_K$ (or those which make up 20% of the estimator value) and coarsen 10% of those cells with smallest $\tilde\eta_K$. By this strategy, we may achieve a prescribed rate of increase of N (or keep it constant in solving nonstationary problems). The fixed fraction strategy is very robust and economical, and is therefore used in most of the examples discussed below.

(iii) Mesh optimization strategy: Use the (heuristic) representation

$$\eta(u_h) = \sum_{K\in\mathbb{T}_h} \eta_K(u_h) \approx \int_\Omega h(x)^2 \Psi(x)\, dx, \tag{3.21}$$

directly for deriving a formula for an optimal mesh-size distribution $h_{\rm opt}(x)$, for details see Bangerth and Rannacher [2]. Corresponding 'optimal' meshes may be constructed by successive hierarchical refinement of an initial coarse mesh or by a sequence of complete remeshings.

3.4. Hyperbolic model case: transport problem. As a simple model case, we consider the scalar transport equation

$$\beta \cdot \nabla u = f \quad \text{in } \Omega, \quad u = g \ \text{ on } \partial\Omega_-, \tag{3.22}$$

on a domain $\Omega \subset \mathbb{R}^2$ with *inflow boundary* $\partial\Omega_- = \{x \in \partial\Omega,\, n \cdot \beta < 0\}$. Accordingly, $\partial\Omega_+ = \partial\Omega \setminus \partial\Omega_-$ is the *outflow boundary*. The transport vector β is assumed as constant for simplicity. Then, the natural solution space is $V = \{v \in L^2(\Omega),\ \beta \cdot \nabla v \in L^2(\Omega)\}$. This problem is discretized using the Galerkin finite element method with *streamline diffusion* stabilization (see Hansbo and Johnson [28] and also Johnson [43]). On quadrilateral meshes $\mathbb{T}_h$, we define subspaces

$$V_h = \{v \in H^1(\Omega),\, v_{|T} \in \widetilde{Q}_1(K),\, K \in \mathbb{T}_h\}$$

consisting of *bilinear* finite elements. The discrete solution $u_h \in V_h$ is defined by

$$(\beta \cdot \nabla u_h - f, \varphi_h + \delta\beta \cdot \nabla\varphi_h) + (n \cdot \beta(g - u_h), \varphi_h)_{\partial\Omega_-} = 0 \quad \forall \varphi_h \in V_h, \tag{3.23}$$

where the stabilization parameter is locally determined by $\delta_K = \alpha h_K$. In this formulation the inflow boundary condition is imposed in the weak sense. This facilitates the use of a duality argument in generating a posteriori error estimates. Let $J(\cdot)$ be a given functional for controlling the error $e = u - u_h$. Following the DWR approach, we consider the corresponding dual problem

$$A_h(\varphi, z) = (\beta \cdot \nabla\varphi, z + \delta\beta \cdot \nabla z) - (n \cdot \beta\varphi, z)_{\partial\Omega_-} = J(\varphi) \quad \forall \varphi \in V, \tag{3.24}$$

which is a transport problem with transport in the negative β-direction. We note that the stabilized bilinear form $A_h(\cdot,\cdot)$ is used in the duality argument in order to achieve an optimal treatment of the stabilization terms; for a detailed discussion of this point see Houston et al. [40]. The error representation reads

$$J(e) = (\beta \cdot \nabla e, z - \varphi_h + \delta\beta \cdot \nabla(z - \varphi_h)) - (n \cdot \beta e, z - z_h)_{\partial\Omega_-},$$

for arbitrary $\varphi_h \in V_h$. This leads us in the following result.

THEOREM 3.7. *For the approximation of the transport problem (3.22) by the finite element scheme (3.23), there holds the a posteriori error estimate*

$$|J(e)| \le \sum_{K \in \mathbb{T}_h} \rho_K \omega_K, \tag{3.25}$$

with the cell residuals ρ_K and weights ω_K defined by

$$\rho_K := \big(\|f - \beta \cdot \nabla u_h\|_K^2 + h_K^{-1}\|n \cdot \beta(u_h - g)\|_{\partial K \cap \partial\Omega_-}^2\big)^{1/2},$$
$$\omega_K := \big(\|z - \varphi_h\|_K^2 + \delta_K^2\|\beta \cdot \nabla(z - \varphi_h)\|_K^2 + h_K\|z - \varphi_h\|_{\partial K \cap \partial\Omega_-}^2\big)^{1/2}.$$

We note that this a posteriori error bound explicitly contains the mesh size h_K and the stabilization parameter δ_K as well. This gives us the possibility to simultaneously adapt both parameters, which is particularly advantageous in capturing sharp layers in the solution.

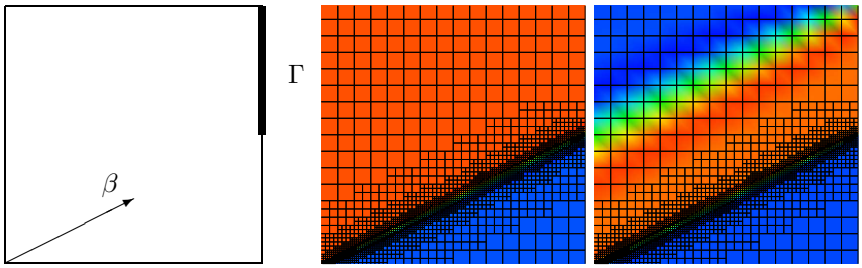

FIGURE 1. *Configuration and grids of the test computation for the model transport problem (3.22) (left), primal solution (middle) and dual solution (right) on an adaptively refined mesh.*

TABLE 1. *Convergence results of the test computation for the model transport problem (3.22).*

L	N	$J(e)$	η	I_{eff}
0	256	2.01e-2	2.38e-2	1.18
2	634	1.09e-2	1.21e-2	1.11
4	1315	6.25e-3	7.88e-3	1.26
6	2050	4.21e-3	5.37e-3	1.27
8	2566	3.90e-3	5.01e-3	1.28
10	3094	3.41e-3	4.71e-3	1.38

A simple thought experiment helps to understand the features of the error estimate (3.25). Let $\Omega = (0,1)^2$ and $f = 0$. We take the functional $J(u) = (1, n \cdot \beta u)_{\partial\Omega_+}$. The corresponding dual solution is $z \equiv 1$, so that $J(e) = 0$. Hence

$$(1, n \cdot \beta u_h)_{\partial\Omega_+} = (1, n \cdot \beta u)_{\partial\Omega_+} = -(1, n \cdot \beta g)_{\partial\Omega_-},$$

which recovers the well-known global conservation property of the scheme.

Next, we take again the unit square $\Omega = (0,1)^2$ and $f = 0$, and consider the case of constant transport $\beta = (1, 0.5)^T$ and inflow data $g(x,0) = 0$, $g(0,y) = 1$. The quantity to be computed is part of the outflow as indicated in Figure 1:

$$J(u) = \int_\Gamma \beta \cdot n u \, ds \,.$$

The mesh refinement is organized according to the *fixed fraction strategy* described above. In Table 1, we show results for this test computation. The corresponding meshes and the primal as well as the dual solution are presented in Figure 1. Notice that there is no mesh refinement enforced of the dual solution along the upper line of discontinuity since here the residual of the primal solution is almost zero. Apparently, this has not much effect on the accuracy of the error estimator.

REMARK 3.8. The results of this simple test show a somewhat counter-intuitive feature of error estimation using the DWR method. The evaluation of the a posteriori error estimator for a functional output $J(u)$ does not require extra mesh

refinement in approximating the dual solution z. It is most economical and sufficiently accurate to compute both approximations u_h as well as z_h on the same (adapted) mesh. This is due to the multiplicative occurrence of residual ρ_K and weight ω_K in the error representation formulas, i.e., in areas where the primal solution u is smooth, and therefore the residual of u_h small, the error in approximating the weight may be large, due to irregularities in z, without significantly affecting the accuracy of the error representation.

3.5. Parabolic model case: heat equation. We consider the heat-conduction problem

$$\partial_t u - \Delta u = f \quad \text{in } Q_T, \quad u_{|t=0} = u^0 \ \text{ in } \Omega, \quad u_{|\partial\Omega} = 0 \ \text{ on } I, \tag{3.26}$$

on a space-time region $Q_T = \Omega \times I$, where $\Omega \subset \mathbb{R}^d$, $d \geq 1$, and $I = [0,T]$; the coefficient a may vary in space. This model is used to describe diffusive transport of energy or certain species concentrations.

The discretization of problem (3.26) uses a Galerkin method in space-time. We split the time interval $[0,T]$ into subintervals $I_n = (t_{n-1}, t_n]$ according to

$$0 = t_0 < ... < t_n < ... < t_N = T, \qquad k_n := t_n - t_{n-1}.$$

At each time level t_n, let $\mathbb{T}_h^n$ be a regular finite element mesh as defined above with local mesh width $h_K = \operatorname{diam}(K)$, and let $V_h^n \subset H_0^1(\Omega)$ be the corresponding finite element subspace with d-linear shape functions. Extending the spatial mesh to the corresponding space-time slab $\Omega \times I_n$, we obtain a global space-time mesh consisting of $(d+1)$-dimensional cubes $Q_K^n := K \times I_n$. On this mesh, we define the global finite element space

$$V_h^k = \big\{ v \in W,\ v(\cdot,t)_{|Q_K^n} \in \tilde{Q}_1(K),\ v(x,\cdot)_{|Q_K^n} \in P_r(I_n)\ \forall\, Q_K^n \big\},$$

where $W = L^2((0,T); H_0^1(\Omega))$ and $r \geq 0$. For functions from this space and their time-continuous analogues, we use the notation

$$v^{n+} = \lim_{t \to t_n + 0} v(t), \quad v^{n-} = \lim_{t \to t_n - 0} v(t), \quad [v]^n = v^{n+} - v^{n-}.$$

The discretization of problem (3.26) is based on a variational formulation which allows the use of piecewise discontinuous functions in time. This method, termed *dG(r) method* (*discontinuous* Galerkin method in time), determines approximations $U \in V_h^k$ by requiring

$$A(U,\varphi) = 0 \quad \forall \varphi \in V_h^k, \tag{3.27}$$

with the semi-linear form

$$A(u,\varphi) \ = \ \sum_{n=1}^{N} \int_{I_n} \big\{ (\partial_t u, \varphi) + (\nabla u, \nabla \varphi) - (f,\varphi) \big\}\, dt + \sum_{n=1}^{N} ([u]_{n-1}, \varphi_{n-1}^+),$$

where $u_0^- = u_0$. We note that the continuous solution u also satisfies equation (3.27) which again implies Galerkin orthogonality for the error $e = u - U$ with respect to the bilinear form $A(\cdot,\cdot)$. Since the test functions $\varphi \in V_h^k$ may be discontinuous at times t_n, the global system (3.27) decouples and can be written in form of a time-stepping scheme,

$$\int_{I_n} \big\{ (\partial_t U, \varphi) + (\nabla U, \nabla \varphi) \big\}\, dt + ([U]^{n-1}, \varphi^{(n-1)+}) = \int_{I_n} (f,\varphi)\, dt, \quad n = 1, ..., N,$$

for all $\varphi \in V_h^n$. In the following, we consider only the lowest-order case $r = 0$, the so-called 'dG(0) method', which is closely related to the backward Euler scheme. For explaining the application of the DWR approach to this situation, we concentrate on the control of the spatial L^2-norm error $\|e^{N-}\|$ at the end time $T = t_N$, corresponding to the error functional

$$J(\varphi) := (\varphi^{N-}, e^{N-})\|e^{N-}\|^{-1}.$$

The corresponding dual problem in space-time reads as

$$\begin{aligned} &\partial_t z - \Delta z = 0 \quad \text{in } \Omega \times I, \\ &z_{|t=T} = \|e^{N-}\|^{-1} e^{N-} \ \text{ in } \Omega, \ \ z_{|\partial\Omega} = 0 \ \text{ on } I. \end{aligned} \tag{3.28}$$

In this situation the abstract error representations (2.9) or (2.10) take the form

$$\begin{aligned} J(e) = \sum_{n=1}^{N} \sum_{K \in \mathbb{T}_h^n} \Big\{ &(R_h^k, z - I_h^k z)_{K \times I_n} + (r_h^k, z - I_h^k z)_{\partial K \times I_n} \\ &- ([U]^{n-1}, (z - I_h^k z)^{(n-1)+})_K \Big\}, \end{aligned} \tag{3.29}$$

with an appropriate approximation $I_h^k z \in V_h^k$ and the local residuals

$$R_{h|K}^k := f - \partial_t U + \Delta U, \qquad r_{h|\Gamma}^k := \begin{cases} -\frac{1}{2}[\partial_n U], & \text{if } \Gamma \subset \partial T \backslash \partial\Omega, \\ 0, & \text{if } \Gamma \subset \partial\Omega. \end{cases}$$

Here, we use the natural interpolation $I_h^k z \in V_h^k$ which is defined by

$$\int_{I_n} I_h^k z(a,t)\, dt = \bar{z}(a), \qquad \bar{z}(x) := \int_{I_n} z(x,t)\, dt, \quad x \in \bar{\Omega},$$

for all nodal points a of the mesh $\mathbb{T}_h^n$. Observing that the time-integrated equation residual $\overline{R_h^k} = \overline{f - \partial_t U + \Delta U}$ as well as the jump-residual r_h^k are constant in time, the a posteriori error representation can be rewritten in the form

$$\begin{aligned} J(e) = \sum_{n=1}^{N} \sum_{K \in \mathbb{T}_h^n} \Big\{ &(f - \overline{f}, z - I_h^k z)_{Q_K^n} + (\overline{R_h^k}, \overline{z} - I_h^k z)_{Q_K^n} \\ &+ (r_h^k, \overline{z} - I_h^k z)_{\partial K \times I_n} - ([U]^{n-1}, (z - I_h^k z)^{(n-1)+})_K \Big\}. \end{aligned} \tag{3.30}$$

¿From this error representation we conclude the following result:

THEOREM 3.9. *For the approximation of the heat conduction problem by the dG(0)-FEM, there holds the a posteriori error estimate*

$$|J(e)| \le \sum_{n=1}^{N} \sum_{K \in \mathbb{T}_h^n} \big\{ \rho_K^{h,n}\, \omega_K^{h,n} + \rho_K^{k,n}\, \omega_K^{k,n} \big\}, \tag{3.31}$$

where the cell residuals and weights can be grouped as follows:
(i) spatial terms:

$$\begin{aligned} \rho_K^{h,n} &:= \big(\|\overline{R_h^k}\|_{K \times I_n}^2 + h_K^{-1} \|r_h^k\|_{\partial K \times I_n}^2 \big)^{1/2}, \\ \omega_K^{h,n} &:= \big(\|\bar{z} - I_h^k z\|_{K \times I_n}^2 + h_K \|\bar{z} - I_h^k z\|_{\partial K \times I_n}^2 \big)^{1/2}, \end{aligned}$$

(ii) temporal terms:

$$\rho_K^{k,n} := \big(\|f-\bar{f}\|^2_{Q_K^n} + k_n^{-1}\|[U]^{n-1}\|^2_K\big)^{1/2},$$
$$\omega_K^{k,n} := \big(\|z-I_h^k z\|_{K\times I_n} + k_n\|(z-I_h^k z)^{(n-1)+}\|^2_K\big)^{1/2}.$$

In the error estimator (3.31) the effect of the space discretization is separated from that of the time discretization. On each space-time cell Q_K^n the indicator $\eta_{K,h}^n := \rho_{K,h}^n \omega_{K,h}^n$ can be used for controlling the spatial mesh width h_K and the indicator $\eta_{K,k}^n := \rho_{K,k}^n \omega_{K,k}^n$ for the time step k_n, i.e., spatial mesh size and time step can be adapted independently. The weights $\omega_{K,h}^n$ and $\omega_{K,k}^n$ are evaluated in the same way as described for the stationary case by post-processing a computed approximation $z_h \in V_h^k$ to the dual solution z. An analogous a posteriori error estimator can also be derived for higher-order time stepping schemes, such as the dG(1) scheme and the cG(1) scheme, the latter being closely related to the popular Crank-Nicolson scheme. For more details, we refer to Bangerth and Rannacher [2] and the literature cited therein. The first complete a posteriori error analysis of dG methods for parabolic problems has been given in a sequence of papers by K. Eriksson and C. Johnson [21–23].

3.5.1. *Numerical test.* The performance of mesh adaptation based on the error identity (3.30) is illustrated by a simple test in two space dimensions where the constructed exact solution represents a smooth rotating bump on the unit square. Figure 3 shows a sequence of adapted meshes at successive times obtained by controlling the spatial L^2-norm error at the end time $t_N = 0.5$. We clearly see the effect of the weights in the error estimator which suppress the influence of the residuals during the initial period. Accordingly, the time step is kept coarse at the beginning and is successively refined when approaching the end time t_N.

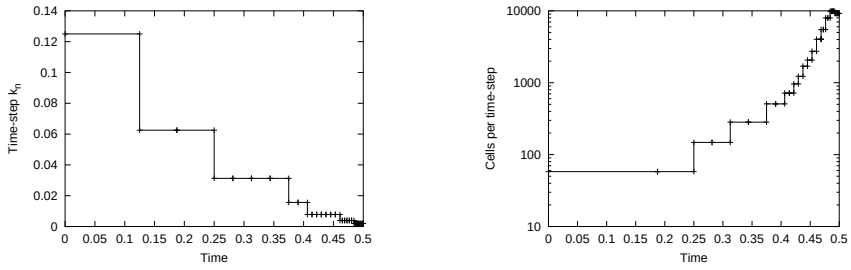

FIGURE 2. *Development of the time-step size (left) and the number N_n of mesh cells (right) over the time interval $I = [0, T = 0.5]$ (from Hartmann [29]).*

4. Application to flow models

4.1. The mathematical models. We only consider continuum mechanical models of gaseous and liquid flows. The basis is the postulated conservation of certain physical quantities describing the state of the flow. These 'conservative' variables are the '(mass) density' ρ, the 'momentum' $m := \rho v$, and the 'total

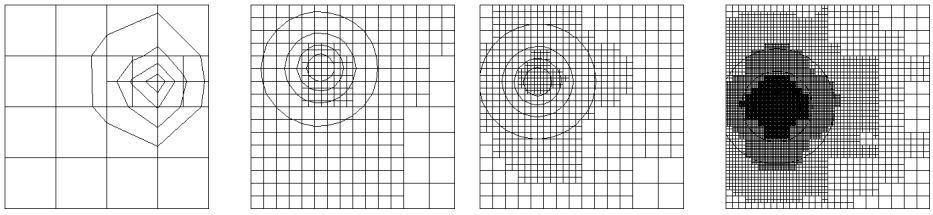

FIGURE 3. *Sequence of refined meshes for controlling the end-time error* $\|e^{N-}\|$ *shown at four consecutive times levels* $t_n = 0.125000, ..., 0.5$ *(from Hartmann [29]).*

energy (density)' $E := \rho e + \frac{1}{2}\rho|v|^2$. The conservation equations read

$$\partial_t \rho + \nabla \cdot (\rho v) = 0 \tag{4.1}$$

$$\partial_t m + \nabla \cdot (m \otimes v) = \nabla \cdot \sigma + \rho f \tag{4.2}$$

$$\partial_t E + \nabla \cdot (Ev) = \rho f \cdot v + \nabla \cdot (\sigma \cdot v) + \rho h - \nabla \cdot q, \tag{4.3}$$

in terms of the 'primitive variables' density ρ, velocity v and temperature θ. Assuming additionally the conservation of torque $x \times m$ implies the symmetry of the 'stress tensor', $\sigma = \sigma^T$. Further 'closing conditions' ('equations of state') reduce the number of unknowns to the number of equations:

- Newtonian fluid ($\mu > 0$, $\lambda = -\frac{2}{3}\mu > 0$ viscosity parameters):

$$\sigma = -pI + \tau, \quad \tau = \mu\{\nabla v + \nabla v^T\} + \lambda \nabla \cdot v I.$$

- Law of ideal gas ($R > 0$ gas constant): $p = p(\rho, \theta) = R\rho\theta$.
- Thermodynamic relations: $e = c_v\theta$, $q = -\kappa(\rho, \theta)\nabla\theta$.

In order to characterize the regime of the flow considered, one uses the 'velocity of sound' with the associated 'Mach number',

$$c(p) := \sqrt{dp/d\rho}, \qquad \mathrm{Ma} := |v|/c(p),$$

and the 'kinematic viscosity' with the associated Reynolds number,

$$\nu := \mu/\rho, \qquad \mathrm{Re} := LU/\nu,$$

where L and U are characteristic scales of length and velocity in the problem.

The decision of 'conservation variables' versus 'primitive variables' for the numerical simulation is a delicate question. There are good arguments for either one of these possibilities. Usually boundary conditions,

$$v_{|\Gamma_{\mathrm{in}}} = v^{\mathrm{in}}, \quad v_{|\Gamma_{\mathrm{rigid}}} = 0, \quad (\nu\partial_n v - pn)_{|\Gamma_{\mathrm{out}}} = P,$$
$$\theta_{|\Gamma_D} = \theta^{\mathrm{wall}}, \quad \partial_n\theta_{|\Gamma_N} = 0,$$

as well as diffusion coefficients are expressed in terms of the primitive variables: $\mu = \mu(\rho, \theta), \kappa = \kappa(\rho, \theta)$. On the other hand, the position of 'shocks' (i.e. jumps or large gradients of the flow variables) are very sensitive with respect to preserving conservation properties. In the case of dominant diffusion and smooth solution both formulations using either 'conservative variables' or 'primitive variables' are theoretically and computationally equivalent. However, in the presence of hydrodynamic 'shocks' the conservative formulation is to be preferred. In the following, we will concentrate the discussion of numerical schemes which are particularly

suited for the two extreme cases of either purely inviscid flow at maximum Mach number $\mathrm{Ma} > 1$ (Euler equations) or diffusion dominated flow at Mach number $0 \leq \mathrm{Ma} \ll 1$ (Navier-Stokes equations).

4.2. Inviscid flows: the Euler equations. Inviscid flow is described by the *Euler equations* for the set of conservative variables $u = \{\rho,\, m,\, E := \rho e + \frac{1}{2}\rho|v|^2\}$. Combining the equations (4.1-4.3) in a suitable way, we obtain the following set of equations:

$$\partial_t \rho + \nabla \cdot (\rho v) = 0, \tag{4.4}$$

$$\partial_t m + \nabla \cdot (m \otimes v + pI) = \rho f, \tag{4.5}$$

$$\partial_t E + \nabla \cdot (Ev + pv) = \rho f \cdot v + \rho h, \tag{4.6}$$

or written in the form of a 'conservation law',

$$\partial_t u + \nabla \cdot F(u) = R(u), \tag{4.7}$$

$$F(u) := \begin{pmatrix} \rho v \\ m \oplus v + pI \\ Ev + pv \end{pmatrix}, \qquad R(u) := \begin{pmatrix} 0 \\ \rho f \\ \rho f \cdot v + \rho h \end{pmatrix}.$$

The material law used is $p = (\gamma - 1)(e - \frac{1}{2}\rho v^2)$. These flows are usually characterized by a larger Mach number $\mathrm{Ma} > 0$, but in the flow region there may also be certain areas of small Ma, such as stagnation points in the flow around blunt bodies. For determining the appropriate boundary conditions along a rigid wall or an artificial numerical boundary Γ with outward normal unit vector n, one has to consider the matrix $B(u,n)$ in $F(u) \cdot n =: B(u,n)u$. Its eigenvalues

$$\lambda_1 = v \cdot n - c, \quad \lambda_2 = v \cdot n, \quad \lambda_3 = v \cdot n + c,$$

determine whether Γ corresponds to 'inflow', where prescription of boundary conditions is necessary, or 'outflow' where nothing should be prescribed.

4.2.1. *Conservative discretization by the dG-FEM.* We discuss the 'discontinuous Galerkin finite element method' or in short the 'dG(r)-FEM' for solving the stationary Euler equations. The parameter $r \in \mathbb{N}_0$ refers to the degree of the polynomials used. Let $\mathbb{T}_h = \{K\}$ be a regular decomposition of the computational domain $\overline{\Omega}$. For each cell $K \in \mathbb{T}_h$ and a given flow field b the in- and out-flow boundary of K are defined by

$$\partial K_- := \{x \in \partial K |\; b(x) \cdot n(x) < 0\}, \quad \partial K_+ := \partial K \setminus \partial K_-.$$

The finite element spaces of degree $r \geq 0$ are given by

$$V_h^{(r)} := \{v_h : Q \to \mathbb{R}^d |\; v_{h|K} \in P_r(K)^d,\; K \in \mathbb{T}_h\}.$$

Starting from the formulation (4.7), we obtain by cellwise integration by parts the variational equation for a smooth solution

$$\sum_{K \in T_h} \{-(F(u), \nabla\varphi)_K + (F(u) \cdot n, \varphi)_{\partial K}\} = 0,$$

for all 'discontinuous' test functions φ. This formulation is completed by appropriate 'jump conditions' for the fluxes $F(u)$ (in- and out-flow conditions) across the

inter-element boundaries. The corresponding Galerkin approximation determines $u_h \in V_h^{(r)}$ by the equations

$$a(u_h)(\varphi_h) := \sum_{K\in T_h} \big\{ -(F(u_h),\nabla\varphi_h)_K + (H(u_h,\hat u_h,n),\varphi_h)_{\partial K}\big\} = 0, \tag{4.8}$$

with appropriate 'numerical fluxes' $H(u_h,\hat u_h,n)$ which satisfy the conditions

$$H(u,u,n) = F(u)\cdot n \quad \text{(consistancy)},$$
$$H(v,w,n) = -H(w,v,-n) \quad \text{(conservation)},$$

where $\hat u_h$ denotes the value of u_h on the neighboring cells. This approximation scheme has several remarkable features:

- The boundary conditions on $\partial\Omega$ are imposed implicitly.
- The local conservation property holds:

$$\int_{\partial K} H(u_h,\hat u_h,n)\,do = 0.$$

- Full Galerkin orthogonality holds:

$$a(u)(\varphi_h) - a(u_h)(\varphi_h) = 0, \quad \varphi_h \in V_h.$$

A simple and popular numerical flux is, for example, the local 'Lax-Friedrichs flux':

$$H_{\rm LF}(u_h,\hat u_h,n) = \tfrac{1}{2}\big\{F(u_h)\cdot n + F(\hat u_h)\cdot n + \alpha(u_h-\hat u_h)\big\}, \tag{4.9}$$

where $\alpha = \max\{\lambda_{max} : B(u_h,n), B(\hat u_h,n)\}$. In the case of solutions with shocks additional damping is required in order to suppress over- and under-shootings. This may be archived by introducing (nonlinear) 'artificial viscosity' (so-called 'shock capturing') of the form

$$s_\epsilon(u_h)(\varphi_h) := \sum_{K\in\mathbb{T}_h} (\epsilon\nabla u_h,\nabla\varphi_h)_K, \qquad \epsilon_{|K} := c_\epsilon h_K^{2-\beta}|\nabla\cdot F(u_h)|_K I_d,$$

where $0\le\beta\le\frac{1}{2}, c_\epsilon > 0$ and $I_d := \mathrm{diag}(0,1,\dots,1)$. With this notation, the stabilized dG scheme for the Euler equations takes the form

$$a_\epsilon(u_h)(\varphi_h) := a(u_h)(\varphi_h) + s_\epsilon(u_h)(\varphi_h) = 0 \quad \forall\varphi_h\in V_h. \tag{4.10}$$

In this case the application of the general theory developed in Section 2 is delicate since the solution of the Euler equations may be discontinuous (shock solution) and is lacking the required degree of regularity for linearization. The corresponding dual problem obtained by linearization about such a solution may not be well-posed. However, this should not prevent us from formally applying the DWR approach even in this situation. Let $J(\cdot)$ by a prescribed output functional defined the exact solution as well as on the finite element spaces. Then, with the solution $u_h\in V_h$ of the discrete Euler equations (4.8), the discrete dual problem is defined by

$$\tilde a_\epsilon'(u_h)(\varphi_h,z_h) = J(\varphi_h) \quad \forall\varphi_h\in V_h. \tag{4.11}$$

where the approximative derivative $\tilde a'(\cdot)(\cdot,\cdot)$ is defined as an appropriate difference quotient. The problem with this linear problem is that it is lacking a thorough existence theory because of its possibly discontinuous coefficients. Nevertheless, practical experience indicates that this problem is less severe. Let us therefore

assume that (4.11) has a solution $z_h \in V_h$. With these two discrete solutions u_h and z_h, we define the following a posteriori error estimator:

$$|J(e)| \approx \tilde{\eta}^{\omega}(u_h) := \Big| \sum_{K\in\mathbb{T}_h} \big\{(R_h,\psi_h)_K + (r_h,\psi_h)_{\partial K} - \epsilon(\nabla u_h\cdot\nabla\psi_h)_K\big\}\Big|, \tag{4.12}$$

where $\psi_h := \tilde{z}_h - z_h$, and the cell and edge residuals are defined by

$$R_{h|K} := -\nabla\cdot F(u_h), \quad r_{h|\partial K} := F(u_h^+)\cdot n - H(u_h^+,u_h^-,n).$$

The corresponding local error indicators have the form

$$\tilde{\eta}_K^{\omega} := |(R_h,\psi_h)_K + (r_h,\psi_h)_{\partial K} - \epsilon(\nabla u_h\cdot\nabla\psi_h)_K|.$$

Here, the approximation $\tilde{z}_h$ to the hypothetical continuous dual solution may again be computed from z_h by patchwise higher-order interpolation as described above.

4.2.2. *An example.* For illustrating the approach described above, we consider the supersonic flow around a BAC3-11 airfoil as originally specified in the AGARD Report AR-303 of 1994, (see Hartmann and Houston [32], and Figure 4). The inflow has $\mathrm{Ma} = 1.2$ and an angle of attack $\alpha = 5^\circ$, with inflow density $\rho^{\mathrm{in}} = 1$ and pressure $p^{\mathrm{in}} = 1$. With these data the solution develops two shocks, one located in front of the leading edge of the airfoil and one originating from the trailing edge. The quantity of interest is the pressure point value

$$J(u) := p(a) = (\gamma-1)(e(a) - \tfrac{1}{2}\rho v(a)^2,$$

at the leading edge of the airfoil which is located in the subsonic region of the flow. Notice that this functional is nonlinear in the primal variables $u = \{\rho, m, E\}$. The stabilization parameters are chosen as $c_\epsilon = 0.03$ and $\beta = 0.1$. The dual solution z is computed by using a higher order method, in this basic case using bi-quadratic elements. The resulting nonlinear algebraic equations are solved by the quasi-Newton method. In general, the numerical fluxes $H(u^+,u^-,n)$ as well as the shock capturing term $s_\epsilon(\cdot)(\cdot)$ are not differentiable. This requires special care in defining the corresponding derivative form $a'_\epsilon(u_h)(\cdot,\cdot)$. For details of this construction, we refer to Hartmann [30, 31].

For comparison, we also use an ad hoc error indicator which uses the residuals of the computed solution without weights,

$$\eta_K^{\mathrm{res}} := \big(h_K^2\|R_h\|_K^2 + h_K\|r_h\|_{\partial K}^2\big)^{1/2}.$$

In view of the a priori knowledge of the characteristics of this flow, we may want to restrict the mesh refinement to a 90°-cone C with opening in the upstream direction and vertex in the airfoil. This is achieved by using the local error indicators

$$\tilde{\eta}_K^{\mathrm{res}} := \begin{cases} \eta_K^{\mathrm{res}}, & \text{if } K\cap C \neq \emptyset, \\ 0, & \text{otherwise.} \end{cases}$$

The results obtained by using the residual error indicators $\tilde{\eta}_K^{\mathrm{res}}$, the modified residual error indicators η_K^{res} and the weighted error indicators $\tilde{\eta}_K^{\omega}$ are shown in Figure 5 and Table 2. It is clearly seen that only the weighted error indicators yield really economical meshes. This can be understood by looking at the isolines of the dual solution shown in Figure 4 which reflect the directions corresponding to the characteristic eigenvalues $v\cdot n \pm c$ and $v\cdot n$. Further, it is seen that shifting the absolute sign in the error estimator in (4.12) under the summation results in a significant

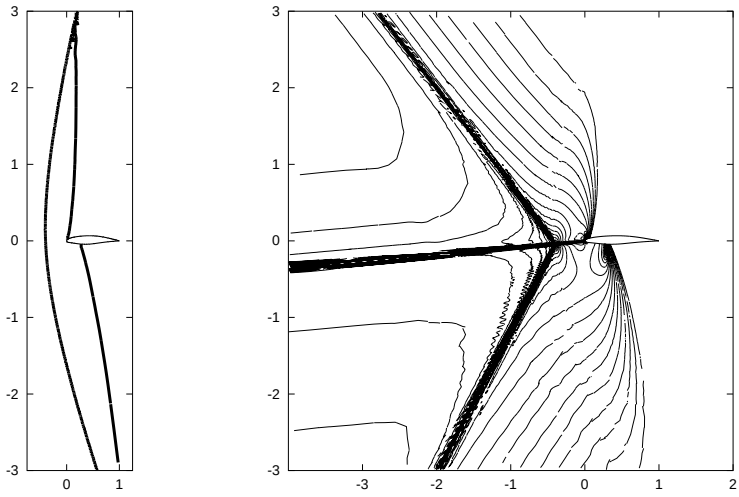

FIGURE 4. *Supersonic flow around the BAC3-11 airfoil:* $\mathrm{Ma} = 1$ *isolines of primal solution (left), isolines of* z_1 *velocity component of dual solution (right) (from Hartmann [30])*

loss of efficiency which is reflected by the behavior of the corresponding effectivity index which growth as $N \to \infty$.

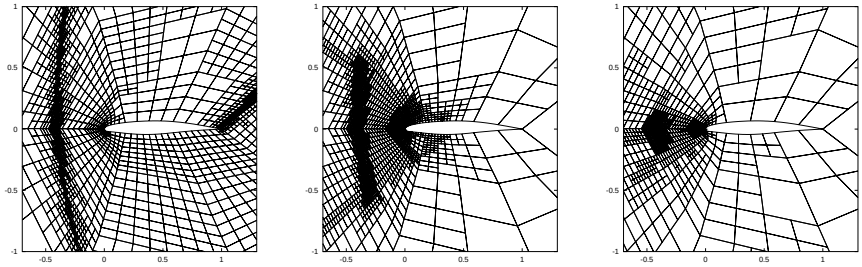

FIGURE 5. *Adapted meshes for computing the pressure point value in a supersonic flow around a BAC3-11 airfoil with about* 1% *error: with* $13,719$ *cells by the residual error indicator (left), with* $9,516$ *cells by the modified residual error indicator (middle), with* $1,803$ *cells by the weighted error indicator (right) (from Hartmann [30]).*

We note that the evaluation of the *a posteriori* error estimate (4.18) involves only the solution of *linearized* problems. Hence, the whole error estimation may amount to a relatively small fraction of the total cost for the solution process. This has to be compared to the usually much higher cost when working on non-optimized meshes.

TABLE 2. *Results of an adaptive finite element computation of the pressure point value in a supersonic flow around a BAC3-11 airfoil (from Hartmann [30]).*

N	$J(u)-J(u_h)$	$\lvert\tilde{\eta}^{\omega}(u_h)\rvert$	I_{eff}	$\sum_{K\in\mathbb{T}_h}\lvert\tilde{\eta}^{\omega}_K(u_h)\rvert$	I_{eff}
348	6.425e-02	2.695e-02	0.42	2.120e-01	3.30
609	2.876e-02	1.389e-02	0.48	1.839e-01	6.39
1065	5.066e-03	7.602e-03	1.50	1.171e-01	23.11
1803	3.042e-03	2.868e-03	0.94	1.028e-01	33.78
3045	1.561e-03	2.801e-03	1.79	1.067e-01	68.39
5643	5.790e-04	5.790e-04	1.00	5.551e-02	95.88

4.3. Viscous flows: the incompressible Navier-Stokes equations. We consider the *stationary* Navier-Stokes system for pairs $u := \{v, p\}$,

$$\mathcal{A}(u) := \left\{ \begin{matrix} -\nu\Delta v + v\cdot\nabla v + \nabla p - f \\ \nabla\cdot v \end{matrix} \right\} = 0 \tag{4.13}$$

with boundary conditions (see Heywood et al. [38])

$$v|_{\Gamma_{\text{rigid}}} = 0, \quad v|_{\Gamma_{\text{in}}} = v^{\text{in}}, \quad \nu\partial_n v - np|_{\Gamma_{\text{out}}} = 0.$$

where Γ_{in}, Γ_{out}, and Γ_{rgid} are the 'inflow', the 'outflow' and the 'rigid' part of the boundary. For this problem, we will consider the full cycle of numerical simulation (see Becker, Heuveline and Rannacher [8]):

- computation of a target quantity $J(u)$ from the solution of
$$\mathcal{A}(u) = 0,$$
- minimization of $J(u)$ w.r.t. some control q quantity under the equation constraint
$$\mathcal{A}(u) + Bq = 0,$$
- determination of the stability of the optimum state $\hat{u}$ by solving the stability eigenvalue problem
$$\mathcal{A}'(\hat{u})u = \lambda\mathcal{M}u.$$

The use of adaptive finite element methods for all three problems can be treated within the same general framework laid out in Section 2.

The finite element approximation of the Navier-Stokes system is based on its variational formulation. To this end, we introduce the solution and spaces

$$L := L^2(\Omega), \quad H := \{v\in H^1(\Omega)^2 : v_{|\Gamma_{\text{in}}\cup\Gamma_{\text{rigid}}}=0\}, \quad V := H\times L,$$

and for arguments $u = \{v, p\}, \varphi = \{\varphi^v, \varphi^p\}$ the semi-linear form ('energy form')

$$a(u)(\varphi) := (\nabla v, \nabla\varphi^v) + (v\cdot\nabla v - f, \varphi^v) - (p, \nabla\cdot\varphi^v) + (\varphi^p, \nabla\cdot v).$$

The variational Navier-Stokes problem then seeks $u \in u^{\text{in}} + V$, such that

$$a(u)(\varphi) = 0 \quad \forall\varphi \in V.$$

The Galerkin finite element discretization uses the Q_1/Q_1-Stokes element, i.e. equal-order d-linear approximation of velocity and pressure (see Figure 6),

$$L_h \subset L, \quad H_h \subset H, \quad V_h := H_h\times L_h,$$

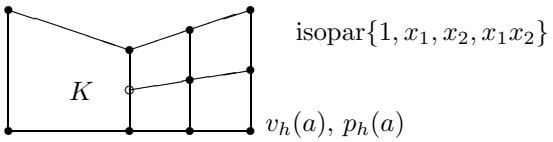

FIGURE 6. *Quadrilateral mesh patch with a 'hanging' node*

defined on quadrilateral or hexahedral meshes. The stability of such a discretization is guaranteed by the so-called 'inf-sup' stability condition (see, e.g., Girault and Raviart [27])

$$\inf_{q_h\in L_h}\sup_{v_h\in H_h}\frac{(q_h,\nabla\cdot v_h)}{\|q_h\|\,\|\nabla v_h\|} =: \beta_h \;\geq\; \beta, \tag{4.14}$$

with an h-independent constant $\beta > 0$. However, the Q_1/Q_1-Stokes element does not satisfy this condition without extra stabilization. Following Hughes et al. [41, 42], this may be achieved within simultaneous 'least-squares' stabilization of pressure-velocity coupling and advection. The stabilized discrete problems seek $u_h \in u_h^{in}+V_h$, such that

$$a_\delta(u_h)(\varphi_h) := a(u_h)(\varphi_h) + (\mathcal{A}(u_h), \mathcal{S}(u_h)\varphi_h)_\delta = 0 \quad \forall\varphi_h \in V_h, \tag{4.15}$$

where

$$\mathcal{S}(u)\varphi := \begin{Bmatrix} v\cdot\nabla\varphi^v + \nabla\varphi^p \\ \nabla\cdot\varphi^v \end{Bmatrix}, \qquad (\varphi,\psi)_\delta := \sum_{K\in\mathbb{T}_h}\delta_K\,(\varphi,\psi)_K.$$

and the stabilization parameter δ_K is chosen adaptively by

$$\delta_K = \alpha\big(\nu h_T^{-2}, \beta\,|v_h|_{K;\infty}h_K^{-1}\big)^{-1}.$$

This is a fully consistent stabilization, i.e., inserting the exact solution yields $a_\delta(u)(\varphi_h) = 0$. This stabilization introduces several terms:

- Stabilization of pressure: $\delta_K(\nabla p_h, \nabla\varphi_h^p)_K$,
- Stabilization of transport: $\delta_K(v_h\cdot\nabla v_h, v_h\cdot\nabla\varphi_h^v)_K$,
- Stabilization of mass conservation: $\delta_K(\nabla\cdot v_h, \nabla\cdot\varphi_h^v)_K$.

4.3.1. *A posteriori error analysis.* Let $J(\cdot)$ be a prescribed (linear) 'error functional' and $z = (z^v, z^p) \in V$ the associated dual solution determined by

$$\nu(\nabla\psi,\nabla z^v) - (\psi, v\cdot\nabla z^v) + (\psi, n\cdot vz^v)_{\Gamma_{\rm out}} + (\psi,\nabla v\,v) = J(\psi), \tag{4.16}$$

for all $\psi = (\psi^v,\psi^p) \in V$. The corresponding 'out-flow boundary condition is of Robin-type, $\{\nu\partial_n z^v + n\cdot\hat{v}z^v - z^p n\}_{|\Gamma_{\rm out}} = 0$. Then, from the general Theorem 2.3, we can infer the following a posteriori error representation (see Becker and Rannacher [12]):

$$J(u) - J(u_h) \;=\; \tfrac{1}{2}\rho(u_h)(z - i_h z) + \;\tfrac{1}{2}\rho^*(u_h,z_h)(u - i_h u) \;+\; \mathcal{R}_h, \tag{4.17}$$

where in this case the cubic remainder $\mathcal{R}_h$ can be bounded as follows:

$$|\mathcal{R}_h| \leq \|e^v\|\,\|\nabla e^v\|\,\|e^{v*}\|_\infty + \mathcal{O}(\delta\|e^v\|),$$

with the errors $e^v := v - v_h$, $e^{v*} := z^v - z_h^v$. Here, the primal residual is given by

$$\rho(u_h)(z - i_h z) := \sum_{K \in \mathbb{T}_h} \big\{ (R_h, z^v - i_h z^v)_K + (r_h, z^v - i_h z^v)_{\partial K} + (z^p - i_h z^p, \nabla \cdot v_h)_K + \dots \big\},$$

with the cell and edge residuals ($[\dots]$ denoting jumps across the cell edges)

$$R_{h|K} := f - \nu \Delta v_h + v_h \cdot \nabla v_h + \nabla p_h,$$

$$r_{h|\Gamma} := \begin{cases} -\frac{1}{2}[\nu \partial_n v_h - n p_h], & \text{if } \Gamma \not\subset \partial\Omega, \\ 0, & \text{if } \Gamma \subset \Gamma_{\text{rigid}} \cup \Gamma_{\text{in}}, \\ -\nu \partial_n v_h + n p_h, & \text{if } \Gamma \subset \Gamma_{\text{out}}. \end{cases}$$

The corresponding dual residual has the form

$$\rho^*(u_h, z_h)(u - i_h u) := \sum_{K \in \mathbb{T}_h} \big\{ (R_h^*, v - i_h v)_K + (r_h^*, v - i_h v)_{\partial K} + (p - i_h p, \nabla \cdot z_h)_K + \dots \big\},$$

with cell and edge residuals

$$R_{h|K}^* := j - \nu \Delta z_h^v - v_h \cdot \nabla z_h^v + \nabla v_h^T z_h^v - \nabla \cdot v_h z_h^v + \nabla z_h^p,$$

$$r_{h|\Gamma}^* := \begin{cases} -\frac{1}{2}[\nu \partial_n z_h^v + n \cdot v_h z_h^v - z_h^p n], & \text{if } \Gamma \not\subset \partial\Omega, \\ 0, & \text{if } \Gamma \subset \Gamma_{\text{rigid}} \cup \Gamma_{\text{in}}, \\ -\nu \partial_n z_h^v - n \cdot v_h z_h^v + z_h^p n, & \text{if } \Gamma \subset \Gamma_{\text{out}}. \end{cases}$$

¿From (4.17), we obtain the practical error estimator

$$\tilde{\eta}_\omega(u_h) := \tfrac{1}{2}\rho(u_h)(\tilde{z}_h - z_h) + \tfrac{1}{2}\rho^*(u_h, z_h)(\tilde{u}_h - u_h), \tag{4.18}$$

where $\tilde{u}_h$ and $\tilde{z}_h$ are approximations to u and z, respectively, obtained by post-processing the Galerkin solutions u_h and z_h, as described above,

$$z - i_h z \approx i_{2h}^{(2)} z_h - z_h, \quad u - i_h u \approx i_{2h}^{(2)} u_h - u_h. \tag{4.19}$$

4.3.2. *A first example: 2D flow around a circular cylinder.* We consider the laminar flow around the cross section of a cylinder in a 2D channel (with slightly displaced vertical position) as shown in Figure 7. This is a standard benchmark problem for which reference solutions are available (Schäfer and Turek [54]).

FIGURE 7. *Configuration of the benchmark problem 'viscous flow around a circular cylinder' with outlets $\Gamma_{1,2}$ for boundary control by pressure variation.*

One of the quantities of physical interest is the drag coefficient defined by

$$J_{\rm drag}(u) = c_{\rm drag} := \frac{2}{\bar U^2 D}\int_S n^T\sigma(v,p)e_x\,{\rm ds},$$

where S is the surface of the cylinder, D its diameter, $\bar U$ the reference inflow velocity, $\sigma(v,p) = \frac{1}{2}\nu(\nabla v+\nabla v^T) + pI$ the stress force acting on S, and e_x the unit vector in the main flow direction. In our example, the Reynolds number is $Re = \bar U^2 D/\nu = 20$, such that the flow is stationary. For evaluating the drag coefficient, one usually uses an equivalent volume-oriented formula, *e.g.*, for the drag:

$$J_{\rm drag}(u) = \frac{2}{\bar U^2 D}\int_\Omega \{\sigma(v,p)\nabla\bar e_x + \nabla\cdot\sigma(v,p)\bar e_x\}\,{\rm dx},$$

where $\bar e_x$ is an extension of e_x to the interior of Ω with support along S. Notice that on the discrete level the two formulas differ. Theory and computation show that the volume formula yields more accurate and robust approximations of the drag coefficient; see Giles et al. [24], and Becker [3]. Since in this case, v as well as p are primal variables the output functional $J_{\rm drag}(\cdot)$ is linear.

Table 3 shows the results of the drag computation, where the effectivity index is again defined by $I_{\rm eff} := |\tilde\eta_\omega(u_h)/J(e)|$. Figure 8 shows refined meshes generated by the 'weighted' error estimator $\tilde\eta_{\rm weight}(u_h)$ and by a (heuristic) 'energy norm' error indicator using only the primal cell residuals,

$$\eta^{\rm res}(u_h) := \Big(\sum_{K\in\mathbb{T}_h}\{h_K^2\|R_h\|_K^2 + h_K\|r_h\|_{\partial K}^2 + h_K^2\|\nabla\cdot v_h\|_K^2\}\Big)^{1/2}.$$

A posteriori error estimates based on this type of residual error indicators have been derived by J. T. Oden et al. [51], Verfürth [56], and Bernardi et al. [14]. In Johnson et al. [45] duality arguments are used to obtain long-term error bounds for the nonstationary Navier-Stokes equations.

TABLE 3. *Results for drag and lift on adaptively refined meshes, error level of* 1% *indicated by bold face (from Becker [3]).*

Computation of drag				
L	N	$c_{\rm drag}$	$\tilde\eta_{\rm drag}$	$I_{\rm eff}$
4	984	5.66058	1.1e−1	0.76
5	2244	5.59431	3.1e−2	0.47
6	**4368**	**5.58980**	1.8e−2	0.58
6	7680	5.58507	8.0e−3	0.69
7	9444	5.58309	6.3e−3	0.55
8	22548	5.58151	2.5e−3	0.77
9	41952	5.58051	1.2e−3	0.76
	∞	5.579535...		

4.3.3. *A second example: 3D flow around a square cylinder.* Next, we consider a 3D version of the above example, namely stationary channel flow around a cylinder with square cross-section. Again the target quantity of the computation is the drag coefficient $c_{\rm drag}$. Table 4 shows the corresponding results compared to those obtained by mesh adaptation based on the residual error indicators $\eta_K^{\rm res}$. The superiority of goal-oriented mesh adaptation is clearly seen. However, one should

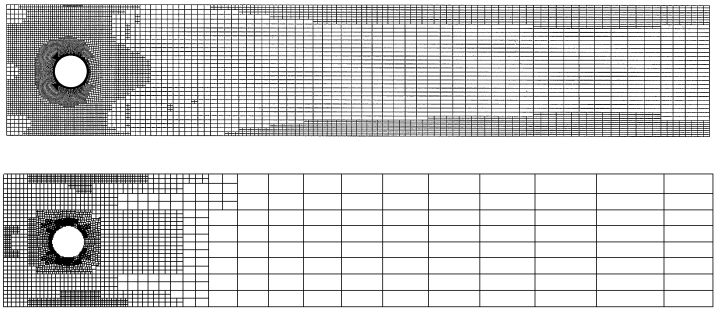

FIGURE 8. *Refined meshes generated by the 'residual error' estimator (top) and by the 'weighted' error estimator (bottom) (from Becker [3]).*

not forget that these specially tuned meshes are not necessarily also appropriate for computing other flow quantities such as the global vortex structure of the flow or the pressure along the shear forces along the walls. For computing these quantities the mesh adaptation has to utilize the corresponding dual solutions.

TABLE 4. *Results of the drag computation: a) with mesh adaptation by 'residual' error indicator, b) with mesh adaptation by 'weighted' error indicator (from Braack and Richter [17])*

N_{res}	c_d	N_{weight}	c_d
$3,696$	12.7888	$3,696$	12.7888
$21,512$	8.7117	$8,456$	9.8262
$80,864$	7.9505	$15,768$	8.1147
$182,352$	7.9142	$30,224$	8.1848
$473,000$	7.8635	$84,832$	7.8282
$-$	$-$	$162,680$	7.7788
∞	7.7730	∞	7.7730

4.4. Optimal flow control. Next, we present some results obtained for the minimization of the drag coefficients by boundary control. The data is chosen such that $\text{Re} = \bar{\text{U}}^2\text{D}/\nu = 40$ for the uncontrolled flow. The drag coefficient c_d is to be minimized by optimally adjusting the pressure prescription q at the secondary outlets $\Gamma_Q = \Gamma_1 \cup \Gamma_2$ (see Figure 7). This means that a state $u \in u^{\text{in}}+V$ is sought, such that

$$J_{\text{drag}}(u) \;\to\; \min,$$

under the constraint

$$a(u)(\varphi) + b(q,\varphi) = (f,\varphi^v) \quad \forall \varphi \in V, \tag{4.20}$$

where the control form is given by

$$b(q,\varphi) := -(q, n\cdot\varphi^v)_{\Gamma_Q}.$$

In Table 5, the values of the drag coefficient on optimized meshes as shown in Figure 10 is compared with results obtained on globally refined meshes. It

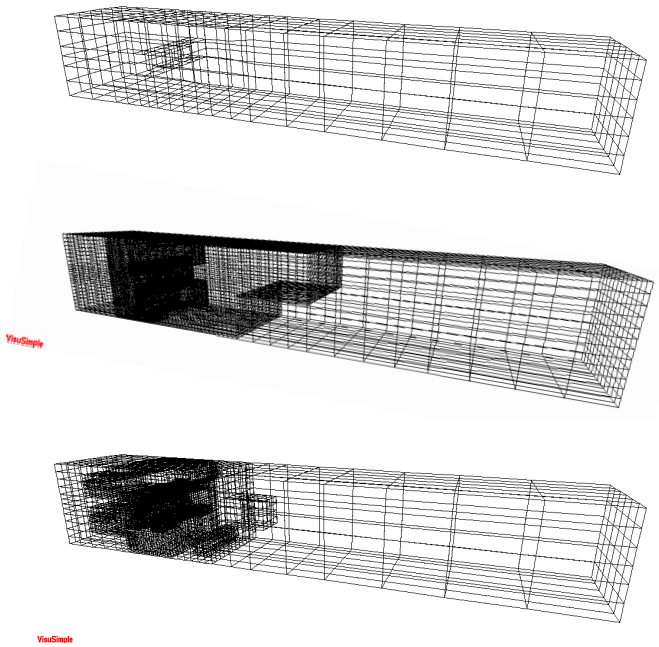

FIGURE 9. *Geometry adapted coarse mesh (top) and refined meshes obtained by the 'energy-norm' (middle) and the 'weighted' error estimator (bottom) (from Becker [4]).*

is clear from these numbers that a significant reduction in the dimension of the discrete model is possible by using appropriately refined meshes. Figure 10 shows streamline plots of the uncontrolled ($q=0$) and the controlled ($q = q^{\rm opt}$) solution and a corresponding 'optimal' mesh.

The locally refined mesh produced by the adaptive algorithm seems to contradict intuition since the recirculation behind the cylinder is not so well resolved. However, due to the particular structure of the optimal velocity field (most of the flow leaves the domain at the control boundary), it might be clear that this recirculation does not significantly influence the cost functional. Instead, a strong local refinement is produced near the cylinder, where the cost functional is evaluated, as well as near the control boundary. It remains the question whether the generated stationary 'optimal' flow is dynamically stable, i.e. can actually be realized in practice.

4.5. Stability eigenvalue problem. For investigating the stability of the stationary optimal state $\hat u = \{\hat v, \hat p\}$ obtained above by the linear stability theory, we have to solve the following non-symmetric eigenvalue problem for $u := \{v, p\} \in V$ and $\lambda \in \mathbb{C}$:

$$-\nu\Delta v + \hat v \cdot \nabla v + v \cdot \nabla \hat v + \nabla p = \lambda v, \quad \nabla \cdot v = 0. \tag{4.21}$$

Its variational form reads

$$a'(\hat u)(u, \varphi) = \lambda m(u, \varphi) \quad \forall \varphi \in V, \tag{4.22}$$

TABLE 5. *Uniform refinement (left) versus adaptive refinement (right) in the drag minimization (from Becker [4])*

Uniform refinement		Adaptive refinement	
N	$J_{\text{drag}}^{\min}$	N	$J_{\text{drag}}^{\min}$
10512	3.31321	1572	3.28625
41504	3.21096	4264	3.16723
164928	3.11800	11146	3.11972

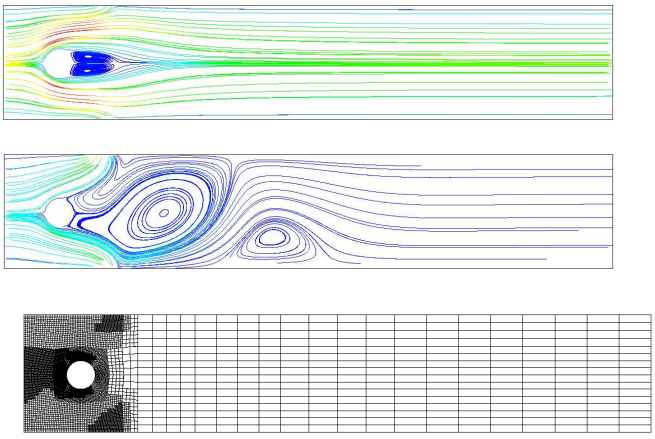

FIGURE 10. *Velocity of the uncontrolled flow (top), the controlled flow (middle) and the corresponding adapted mesh (bottom) (from Becker [4])*

where $m(u,\varphi) := (v,\varphi^v)$. The associated 'adjoint' eigenvalue problem determines $v^* \in V$ and $\lambda^* = \bar{\lambda} \in \mathbb{C}$, such that

$$\nu(\nabla\psi,\nabla v^*) - (\psi,\hat{v}\cdot\nabla v^*) + (\psi, n\cdot\hat{v}v^*)_{\Gamma_{\text{out}}} + (\psi,\nabla\hat{v}\,v) = \lambda^*(\psi,v^*), \tag{4.23}$$

for all $\psi \in V$. The dual eigenpair has to satisfy Robin-type outflow boundary conditions, $\{\nu\partial_n v^* + n\cdot\hat{v}v^* - p^*n\}_{|\Gamma_{\text{out}}} = 0$. ¿From the general Theorem 2.6, we obtain the eigenvalue error estimator

$$|\lambda^{\text{crit}} - \lambda_h^{\text{crit}}| \le \sum_{K\in\mathbb{T}_h} \{\hat{\eta}_K + \eta_K^{\lambda}\} + \mathcal{R}_h. \tag{4.24}$$

where the cell error indicators $\hat{\eta}_K = \hat{\rho}_K(\hat{u}_h)\hat{\omega}_K$ and $\eta_K^{\lambda} = \rho_K(u_h)\omega_K$ represent the errors due to the approximation of the optimal base flow $\hat{u} = \{\hat{v},\hat{p}\}$ and the approximation of the corresponding eigenpair $\{u,\lambda\}$, respectively. For instance, the primal eigenvalue error indicators are obtained from the residual term

$$\rho_K(u_h)(u^*-\psi_h) := \sum_{K\in\mathbb{T}_h} \{(R_h,\hat{v}^*-\psi_h)_K + (r_h,\hat{v}^*-\psi_h)_{\partial K} + (\hat{p}^*-\chi_h,\nabla\cdot\hat{v}_h)_K + \dots\},$$

with the cell and edge residuals defined by

$$R_{h|K} := \lambda v_h + \nu\Delta v_h - v_h\cdot\nabla v_h - \nabla p_h,$$
$$r_{h|\Gamma} := \begin{cases} -\frac{1}{2}[\nu\partial_n v_h - np_h], & \text{if } \Gamma \not\subset \partial\Omega, \\ 0, & \text{if } \Gamma \subset \Gamma_{\rm rigid}\cup\Gamma_{\rm in}, \\ \nu\partial v_h + np_h, & \text{if } \Gamma \subset \Gamma_{\rm out}. \end{cases}$$

This leads us to the following criterion for balancing linearization and discretization error:

$$\sum_{K\in\mathbb{T}_h} \hat\eta_K \le \sum_{K\in\mathbb{T}_h} \eta_K^\lambda. \tag{4.25}$$

This criterion together with the fixed-fraction strategy described above has been used in the computation of the critical eigenvalues of the optimum state $\hat u$. Figure 11 shows adapted meshes for computing the optimum stationary state and the corresponding critical eigenvalue $\lambda^{\rm crit}$. We see that the eigenvalue computation requires more global mesh refinement. This is reflected by the results shown in Figure 12. On coarser meshes, such as used in the optimization process, the error due to the linearization about the wrong base solution $\hat u_h$ dominates the error due to the discretization of the eigenvalue problem, but on more globally refined meshes the picture changes and the linearization error falls below the discretization error. Still the meshes obtained by this adaptation process are more economical than simply using the meshes generated by the plain residual-based error estimator.

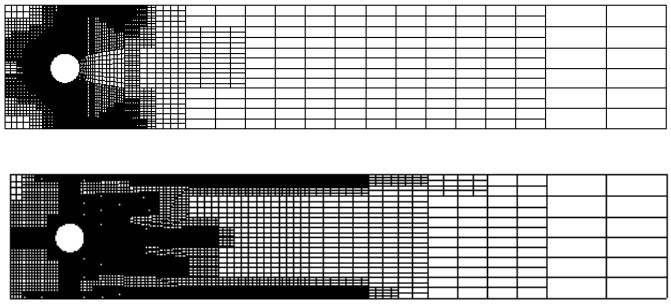

FIGURE 11. *Meshes obtained by the error estimators for the drag minimization (top) and the eigenvalue computation (bottom) (from Heuveline and Rannacher [36])*

4.6. Heat-driven compressible flow. Next, we consider low-Mach number viscous flows which are driven by temperature gradients. Such conditions often occur in chemically reactive flows and are characterized by hydrodynamically incompressible behavior. In view of the rather stiff coupling of total pressure and momentum the treatment of such flows requires a methodology which is oriented at the incompressible limit case, i.e., the pressure as a primary variable is computed from the momentum equations and the density is obtained as a secondary variable from the gas law. Otherwise small errors in the temperature approximation could result in disastrous errors in the velocity. Accordingly the total pressure is split into a small spatially variable 'hydrodynamical' component $p_{\rm hyd}$ which is determined

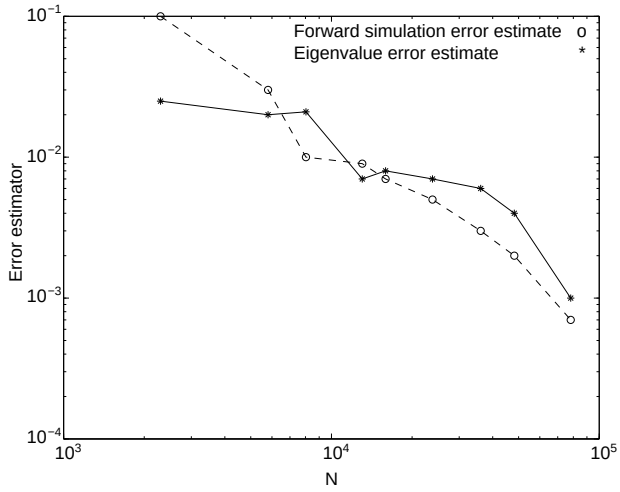

FIGURE 12. *The size of the two components of the error estimator* $\eta_h^\lambda(\hat{u}_h, \hat{u}_h^*, u_h, u_h^*, \lambda_h)$ *, i.e. the errors in the base solution and the eigenvalue approximation (from Heuveline and Rannacher [36])*

by the momentum equation, and a large spatially constant 'thermodynamical' component $P_{\rm th}$ which enters the gas law,

$$p_{\rm tot} = p_{\rm hyd} + P_{\rm th}, \quad \rho \approx \frac{P_{th}}{R\theta}. \tag{4.26}$$

This ansatz leads us to the following 'low-Mach number' formulation of the 'compressible' Navier-Stokes equations:

$$\nabla \cdot v - \theta^{-1}\partial_t\theta - \theta^{-1} v \cdot \nabla\theta = -p_{\rm th}^{-1}\partial_t P_{\rm th}, \tag{4.27}$$

$$\rho\partial_t v + \rho v \cdot \nabla v + \nabla \cdot \tau + \nabla p_{hyd} = \rho g, \tag{4.28}$$

$$\rho c_p \partial_t\theta + \rho c_p v \cdot \nabla\theta - \nabla \cdot (\kappa\nabla\theta) = \partial_t P_{\rm th} + \rho h, \tag{4.29}$$

in which temperature sources by mechanical effects are neglected,

$$\sigma : \nabla v \approx 0, \quad \partial_t p_{\rm hyd} + v \cdot \nabla p_{\rm hyd} \approx 0.$$

The stress tensor is given by $\tau = -\mu\{\nabla v + (\nabla v)^T - \frac{2}{3}(\nabla \cdot v)I\}$. The thermodynamic pressure $P_{\rm th}$ is determined by

$$P_{\rm th} \equiv P_{{\rm th}|\Gamma_{\rm out}} \quad \text{(open flow domain)},$$
$$\partial_t P_{\rm th} = \frac{P_{\rm th}}{|\Omega|}\int_\Omega \theta^{-1}(\partial_t\theta + v \cdot \nabla\theta)\, do \quad \text{(closed box)}.$$

We note that all these formal simplifications of the original conservation equations are not really essential for the numerical methods based on this formulation. What matters is that the pressure and not the density is treated as a primal variable and that the flow is in the low-Mach number regime.

Assuming that the temperature variations about some mean value θ_0 are small, i.e., $|\theta - \theta_0| \ll 1$ and $|\rho - \rho_0| \ll 1$, we can freeze the viscosity at $\mu \approx \mu(\theta_0)$ and

obtain the so-called Boussinesq approximation:

$$\begin{aligned} \nabla \cdot v &= 0 \\ \partial_t v + v \cdot \nabla v - \nu \Delta v + \nabla p &= \beta \theta g \\ c_p \rho_0 \partial_t \theta + c_p \rho_0 v \cdot \nabla \theta - \nabla \cdot (\kappa \nabla \theta) &= 0 \end{aligned}$$

¿From this, we arrive at the classical Navier-Stokes equations by additionally assuming isothermal flow and constant density.

The variational formulation of (4.27 - 4.29) uses the following semilinear form defined for triples $u = \{p, v, \theta\}$, $\varphi = \{\varphi^\rho, \varphi^v, \varphi^\theta\}$:

$$\begin{aligned} A(u)(\varphi) \;:=\; & (\nabla \cdot v - \theta^{-1} v \cdot \nabla \theta, \varphi^\rho) + (\rho v \cdot \nabla v, \varphi^v) - (\tau, \nabla \varphi^v) - (p, \nabla \cdot \varphi^v) \\ & - (p, \nabla \cdot \varphi^v) - (\rho g, \varphi^v) + (\rho v \cdot \nabla \theta, \varphi^\theta) + (\kappa \nabla \theta, \nabla \varphi^\theta)\,. \end{aligned}$$

Further, we define the functional

$$F(\varphi) \;:=\; -(\rho_0 g, \varphi^v).$$

The natural solution spaces are

$$\hat{V} = L^2(\Omega)/\mathbb{R} \times H^1(\Omega)^2 \times H^1(\Omega), \quad V := L^2(\Omega)/\mathbb{R} \times H^1_0(\Omega)^2 \times H^1_0(\Gamma_D; \Omega),$$

where $H^1_0(\Gamma_D; \Omega) := \{\theta \in H^1(\Omega),\, \theta = 0 \text{ on } \Gamma_D\}$. With this notation, the variational form of (4.27 - 4.29) seeks $u = \{p, v, \theta\} \in V + \hat{u}$, with $\hat{u} := \{0, 0, \hat{\theta}\}$, satisfying

$$A(u)(\varphi) = F(\varphi) \quad \forall \varphi \in V, \tag{4.30}$$

where ρ is considered as a (nonlinear) coefficient determined by the temperature through the equation of state $\rho = P_{\text{th}}/R\theta$. For more details on the derivation of this model, we refer to Braack and Rannacher [16], and the literature cited therein. Here, we assume again that (4.30) possesses a solution $u \in \hat{V}$.

The discretization of the system (4.30) uses again the continuous Q_1-finite element for all unknowns and employs least-squares stabilization for the velocity-pressure coupling as well as for the transport terms. We do not explicitly state the corresponding discrete equations since they have an analogous structure, as already seen in the preceding example of the incompressible Navier-Stokes equations. The derivation of the related adjoint problem and the resulting *a posteriori* error estimates follow the same line of argument. For economy reasons, we do not use the full Jacobian of the coupled system in setting up the adjoint problem, but only include its dominant parts. The same simplification is used in the nonlinear iteration process. For details, we refer to Braack and Rannacher [16] and Becker et al. [6]. Below, we again use the mesh-dependent inner product and norm:

$$(v, \psi)_h := \sum\nolimits_{K \in \mathbb{T}_h} \delta_K\, (v, \psi)_K, \quad \|v\|_h = (v, v)_h^{1/2},$$

with some stabilization parameters δ_K. The discrete problems seek triples $u_h = \{p_h, v_h, \theta_h\} \in V_h + \hat{u}_h$, satisfying

$$A_h(u_h)(\varphi_h) = F(\varphi_h) \quad \forall \varphi_h \in V_h, \tag{4.31}$$

with the stabilized form

$$A_h(u_h)(\varphi_h) := A(u_h)(\varphi_h) + (A(u_h) - F, S(u_h)\varphi_h)_h.$$

Here, the operator $A(u_h)$ is the generator of the form $A(u_h)(\cdot)$, and the operator $S(u_h)$ in the stabilization term is chosen according to

$$S(u_h) := \begin{bmatrix} 0 & \operatorname{div} & 0 \\ \nabla & \rho_h v_h \cdot \nabla + \nabla \cdot \mu \nabla & 0 \\ -\theta_h^{-1} v_h \cdot \nabla & 0 & \rho_h v_h \cdot \nabla + \nabla \cdot \kappa \nabla \end{bmatrix}.$$

As on the continuous level, the discrete density is determined by the temperature through the equation of state $\rho_h := P_{\mathrm{th}}/R\theta_h$.

4.6.1. *The algebraic problems.* In order to convert the discrete variational problem (4.15) into an algebraic system, we introduce a nodal basis $\{\varphi_h^i\}_{i=1,\dots,N}$ of $\mathcal{V}_h$, where $N := \dim \mathcal{V}_h$. Then, the coefficients $x = (x_i)_{i=1}^N$ in the ansatz

$$u_h = \sum_{i=1}^{N} x_i \varphi_h^i$$

are determined by the nonlinear algebraic system

$$a_\delta\big(\textstyle\sum_{i=1}^{N} x_i \varphi_h^i)(\varphi_h^i\big) = 0, \quad i = 1, \dots, N.$$

This may be solved by a Newton or a quasi-Newton iteration. For reducing the costs, the Jacobian of the coupled system is usually simplified by neglecting certain of the sub-matrices representing the coupling between flow and temperature. Ordering the unknowns in a physically block-wise manner, i.e., marching through the set of nodal points and attaching to each node the corresponding submatrix containing the unknowns of all physical quantities, we obtain 'nodal matrices' $\mathcal{A}_{ij}$ of the form

$$\mathcal{A}_{ij} = \begin{bmatrix} B_{pp} & B_{pv} & B_{p\theta} \\ B_{vp} & B_{vv} & B_{v\theta} \\ B_{\theta p} & B_{\theta v} & B_{\theta\theta} \end{bmatrix} \quad \approx \quad \widetilde{\mathcal{A}}_{ij} = \begin{bmatrix} B_{pp} & B_{pv} & 0 \\ B_{vp} & B_{vv} & 0 \\ 0 & 0 & B_{\theta\theta} \end{bmatrix}$$

where the indices p, v, θ indicate the corresponding contributions.

Remark 4.1. The obvious simplification of the above system by decoupling of the flow variables $\{p, v\}$ from the temperature θ (or other state variables describing for example chemical reactions) within an operator splitting approach is not appropriate due to the strong influence of the temperature on the flow field and vice versa.

4.6.2. *A posteriori error analysis.* We introduce the following notation for the cell residuals of the solution $u_h = \{p_h, v_h, \theta_h\}$ of (4.31):

$$\begin{aligned} R^p_{h|K} &= \nabla \cdot v_h - \theta_h^{-1} v_h \cdot \nabla \theta_h, \\ R^v_{h|K} &= \rho_h v_h \cdot \nabla v_h - \nabla \cdot (\mu \nabla v_h) + \nabla p_h + (\rho_0 \rho_h) g, \\ R^\theta_{h|K} &= \rho_h v_h \cdot \nabla \theta_h - \nabla \cdot (\kappa \nabla \theta_h) - f_\theta. \end{aligned}$$

Further, we define the edge residuals

$$r^v_{h|\Gamma} := \begin{cases} -\frac{1}{2}[\nu\partial_n v_h - p_h n], & \text{if } \Gamma \not\subset \partial\Omega, \\ 0, & \text{if } \Gamma \subset \Gamma_{\rm rigid} \cup \Gamma_{\rm in}, \\ -(\nu\partial_n v_h - p_h n), & \text{if } \Gamma \subset \Gamma_{\rm out}, \end{cases}$$

$$r^\theta_{h|\Gamma} := \begin{cases} -\frac{1}{2}[\kappa\partial_n \theta_h], & \text{if } \Gamma \not\subset \partial\Omega, \\ 0, & \text{if } \Gamma \subset \partial\Omega_{\rm D}, \\ -\kappa\partial_n \theta_h, & \text{if } \Gamma \subset \partial\Omega_{\rm N}, \end{cases}$$

with $[\cdot]$ again denoting the jump across a cell edge Γ. These quantities will be needed below for defining the *a posteriori* error estimator. Using this notation the stabilizing part in $A_h(\cdot)(\cdot)$ can be written in the form

$$\begin{aligned}(A(u_h), S(u_h)\varphi)_h \ &= (R^p_h, \nabla\cdot\psi)_h + (R^v_h, \nabla\xi + \rho_h v_h\cdot\nabla\psi + \nabla\cdot(\mu\nabla\psi))_h \\ &\quad + (R^\theta_h, \rho_h v_h\cdot\nabla\theta + \nabla\cdot(\kappa\nabla\theta) - \theta_h^{-1} v_h\cdot\nabla\xi)_h\,,\end{aligned}$$

for $\varphi = \{\xi, \psi, \theta\}$. These terms comprise stabilization of the stiff velocity-pressure coupling in the low-Mach-number case and stabilization of transport in the momentum and energy equation case as well as the enforcement of mass conservation. The parameters $\delta_K = \{\delta^p_K, \delta^v_K, \delta^\theta_K\}$ may be chosen differently in the three equations. The stability of this discretization has been investigated in Braack [15].

Now, we turn to the question of *a posteriori* error estimation in the scheme (4.31). Let $J(\cdot)$ again be a (for simplicity) linear functional defined on $\hat V$ for evaluating the error $e = \{e^p, e^v, e^\theta\}$. As in the previous section on incompressible flow, the adjoint problem is again set up using a reduced Jacobian in order to guarantee existence of the adjoint solution. Accordingly, we consider the h-dependent adjoint problem

$$\tilde A'_h(u)(\varphi, z) := A'(u)(\varphi, z) + (S(u)\varphi, S(u)z)_h = J(\varphi) \quad \forall\varphi\in\hat V. \tag{4.32}$$

Then, the general Theorem 2.3 suggests the following error estimator:

$$|J(e)| \approx \eta^\omega(u_h) := \sum_{K\in\mathbb{T}_h}\sum_{\alpha\in\{p,v,\theta\}} \rho^\alpha_K\omega^\alpha_K, \tag{4.33}$$

where the residual terms and weights are defined by

$$\begin{aligned}
\rho^p_K &:= \|R^p_h\|_K, \\
\omega^p_K &:= \|z^p - i_h z^p\|_K + \delta^p_K\|S^p(u_h)(z^p - i_h z^p)\|_K, \\
\rho^v_K &:= \|R^v_h\|_K + h_K^{-1/2}\|r^v_h\|_{\partial K}, \\
\omega^v_K &:= \|z^v - i_h z^v\|_K + h_K^{1/2}\|z^v - i_h z^v\|_{\partial K} + \delta^v_K\|S^v(u_h)(z^v - i_h z^v)\|_K, \\
\rho^\theta_K &:= \|R^\theta_h\|_K + h_K^{-1/2}\|r^\theta_h\|_{\partial K}, \\
\omega^\theta_K &:= \|z^\theta - i_h z^\theta\|_K + h_K^{1/2}\|z^\theta - i_h z^\theta\|_{\partial K} + \delta^\theta_K\|S^\theta(u_h)(z^\theta - i_h z^\theta)\|_K.
\end{aligned}$$

Here, we assume for simplicity that viscosity μ and heat conductivity κ are determined by the reference temperature θ_0, i.e., these quantities are not included in the linearization process. This is justified because of their relatively small variation with θ. Furthermore, the explicit dependence of the stabilization parameters δ_K

on the discrete solution u_h is neglected. The weighted error estimator $\eta^\omega(u_h)$ will be compared to the usual 'residual' error estimator

$$\eta^{\rm res}(u_h) := \Big(\sum_{K\in\mathbb{T}_h} \sum_{\alpha\in\{p,v,\theta\}} |\rho_K^\alpha|^2 \Big)^{1/2}.$$

The weights in the *a posteriori* error estimate (4.33) are again evaluated by solving the adjoint problem numerically on the current mesh and approximating the exact adjoint solution z by patch-wise higher-order interpolation of its computed approximation $\tilde{z}_h$, as described above. For illustration, we state the strong form of the adjoint problem (suppressing terms related to the least-squares stabilization) used in our test computations:

$$\begin{aligned} \nabla\cdot z^v &= j^p, \\ -\rho(v\cdot\nabla)z^v - \nabla\cdot\mu\nabla z^v - \rho\nabla z^p &= j^v, \\ \theta^{-1}v\cdot\nabla z^p + \theta^{-2}v\cdot\nabla\theta\cdot z^p - \rho v\cdot\nabla z^\theta - \ c_p^{-1}\nabla\cdot(\lambda\nabla z^\theta) - (Df^\theta)_\theta z^\theta &= j^\theta, \end{aligned}$$

where $\{j^p, j^v, j^\theta\}$ is a suitable function representation of the error functional $J(\cdot)$. This system is closed by appropriate boundary conditions.

Remark 4.2. The most important feature of the *a posteriori* error estimate (4.39) is that the local cell residuals related to the various physical effects governing flow and transfer of temperature are systematically weighted according to their impact on the error quantity to be controlled. For illustration, let us consider control of the mean velocity

$$J(u) = |\Omega|^{-1}\int_\Omega v\,{\rm dx}.$$

Then, in the adjoint problem the right-hand sides j^p and j^T vanish, but because of the coupling of the variables all components of the adjoint solution $z=\{z^p, z^v, z^\theta\}$ will be nonzero. Consequently, the error term to be controlled is also affected by the cell residuals of the mass-balance and the energy equation. This sensitivity is quantitatively represented by the weights involving z^p and z^θ.

4.6.3. *Numerical example: heat-driven cavity.* As a proto-typical model situation, we consider the benchmark problem 'heat-driven cavity' (Becker and Braack [5]). The flow in a square box with side length $L=1$ is driven by a temperature difference of $\theta_h - \theta_c = 720\,K$ between the left ('hot') and the right ('cold') wall under the action of gravity g in the negative y-direction. The boundary conditions are

$$v_{|\partial\Omega} = 0, \qquad \partial_n\theta_{|\Gamma_N} = 0, \quad \theta_{|\Gamma_{hot}} = \theta_h, \quad \theta_{|\Gamma_{cold}} = \theta_c.$$

Sutherland's viscosity law is used,

$$\mu(\theta) \;=\; \mu^*\Big(\frac{\theta}{\theta^*}\Big)^{1/3}\frac{\theta^*+110.5\,K}{\theta+110.5\,K}, \qquad \kappa(\theta)=\mu(\theta)/{\rm Pr},$$

where $\theta^* = 273\,K$ and $\mu^* = 1.68\cdot10^{-5}$kg/ms. With the Prandtl number ${\rm Pr}=0.71$, the Rayleigh number is determined by

$${\rm Ra} \;=\; {\rm Pr}\,g\Big(\frac{\rho_0 L}{\mu_0}\Big)^2\frac{\theta_h-\theta_c}{\theta_0} \sim 10^6.$$

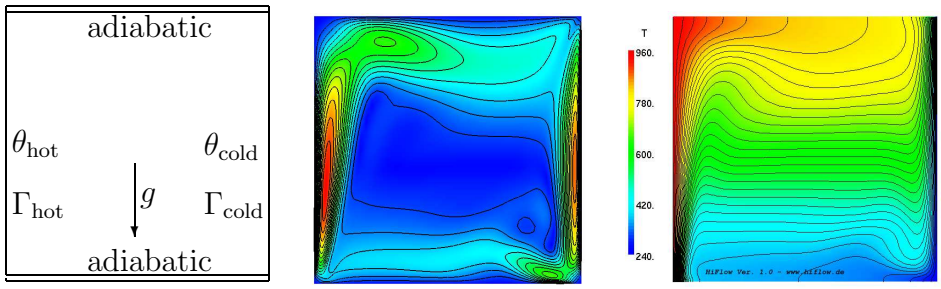

FIGURE 13. *Configuration of 'heat-driven cavity' benchmark (left), velocity norm isolines (middle) and temperature isolines (right) (from Becker and Rannacher [12])*

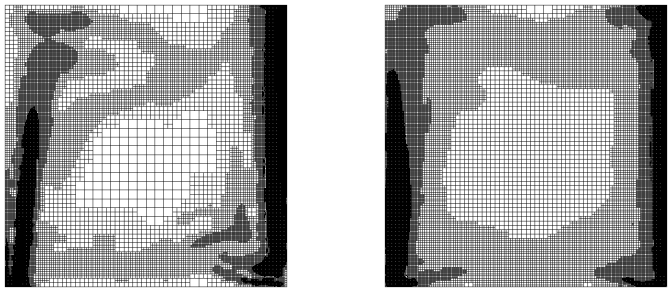

FIGURE 14. *Adapted meshes with about* $58,000$ *cells for the 'heat-driven cavity' for a* 1% *error: 'residual' (left) and 'weighted' error estimator (right) (from Becker and Rannacher [12]).*

The quantity of interest is the average Nusselt number along the cold wall,

$$J(u) = \text{Nu} := \frac{\text{Pr}}{0.3\mu_0\theta_0} \int_{\Gamma_{\text{cold}}} \kappa \partial_n \theta \, ds.$$

¿From the velocity-norm and temperature plots in Figure 13, we see that the temperature boundary layer is strictly attached to the hot wall while the region of large velocity gradients extends more into the flow domain. This raises the question which of these layers has to be resolved by mesh refinement in order to get the best accuracy in the average Nusselt number? This question is answered by the mesh plots in Figure 14. The weighted error estimator orientates the mesh refinement at the temperature boundary layers while the residual error estimator puts more emphasis on the velocity behavior. Which one of these strategies is more effective, is clearly seen in Figure 15.

4.7. Chemically reactive flows. Next, we extend the 'low Mach number' flow model (4.27 - 4.29) by including chemical reactions. In this case the equations of mass, momentum and energy conservation are supplemented by the equations of

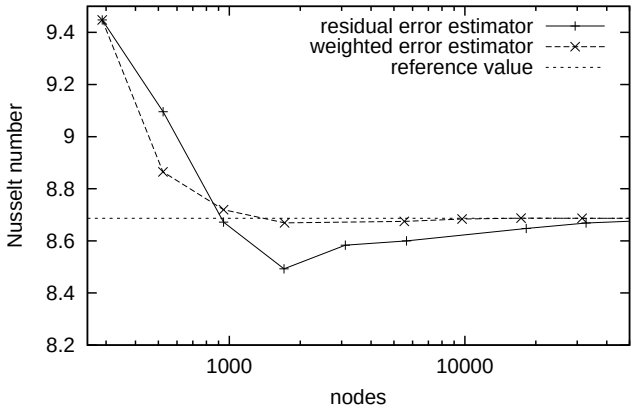

FIGURE 15. *Efficiency of computing the Nusselt number using the 'residual' (symbol +) and the 'weighted error estimator' (symbol ×) (from Becker and Rannacher [12]).*

species mass conservation:

$$\nabla \cdot v - \theta^{-1} v \cdot \nabla\theta - M^{-1} v \cdot \nabla M = 0, \tag{4.34}$$

$$(\rho v \cdot \nabla) v + \nabla \cdot \tau + \nabla p = \rho f_e, \tag{4.35}$$

$$\rho v \cdot \nabla\theta - c_p^{-1} \nabla \cdot (\lambda \nabla\theta) = c_p^{-1} f_t(\theta, w), \tag{4.36}$$

$$\rho v \cdot \nabla w_i - \nabla \cdot (\rho D_i \nabla w_i) = f_i(\theta, w), \quad i = 1, \ldots, n. \tag{4.37}$$

In this case the gas law takes the form

$$\rho = \frac{P_{\text{th}} M}{R\theta}, \tag{4.38}$$

with the mean molar mass $M := (\sum_{i=1}^{n} w_i/M_i)^{-1}$ and the species mole masses M_i (see Braack and Rannacher [16] for more details of this model).

Owing to exponential dependence on temperature (Arrhenius' law) and polynomial dependence on w, the source terms $f_i(\theta, w)$ are highly nonlinear. In general, these zero-order terms lead to a coupling between all chemical species mass fractions. For robustness the resulting system of equations is to be solved by an implicit and fully coupled process that uses strongly adapted meshes. The discretization of the full flow system again uses continuous Q_1-finite elements for all unknowns and employs least-squares stabilization for the velocity-pressure coupling as well as for all the transport terms. We do not state the corresponding discrete equations since they have the same structure as seen before. The derivation of the related (linearized) adjoint problem corresponding to some (linear) functional $J(\cdot)$ and the resulting *a posteriori* error estimates follows the same line of argument. Again, one may use a simplified Jacobian of the coupled system in setting up the adjoint problem (for details see Braack and Rannacher [16]. The resulting *a posteriori* error estimator has the same structure as that in (4.33), only that additional terms occur due to the balance equations for the chemical species:

$$|J(e)| \approx \sum_{K \in \mathbb{T}_h} \sum_{\alpha \in \{p,v,\theta,w_i\}} \rho_K^\alpha \omega_K^\alpha, \tag{4.39}$$

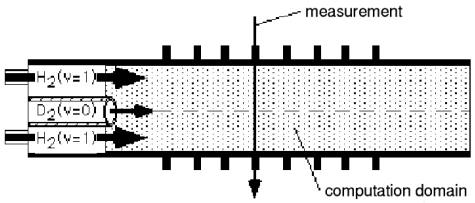

FIGURE 16. *Configuration of the chemical flow reactor with axisymmetric symmetry of domain and flow.*

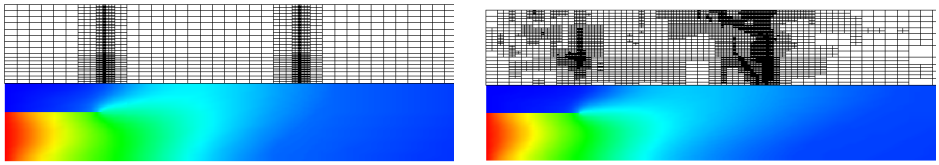

FIGURE 17. *Mass fraction of* $D_2^{(1)}$ *in the flow reactor computed on a tensor-product mesh (left) and on a locally adapted mesh (right) (from Becker et al. [7])*

with the chemistry-related additional residual terms and weights

$$\rho_K^{w_i} := \|R^{w_i}(u_h)\|_K + h_K^{-1/2}\|r^{w_i}(u_h)\|_{\partial K}\,, \quad i = 1,\dots,n,$$
$$\omega_K^{w_i} := \|z^{w_i} - i_h z^{w_i}\|_K + h_K^{1/2}\|z^{w_i} - i_h z^{w_i}\|_{\partial K} + \delta_K^{w_i}\|S^{w_i}(u_h)(z^{w_i} - i_h z^{w_i})\|_K\,.$$

The weights in the *a posteriori* error estimate (4.39) are again evaluated in the same way as described above.

4.7.1. *Numerical example: flow reactor.* We consider a chemical flow reactor (see Figure 16) for determining the reaction velocity of the heterogeneous relaxation of vibrationally excited hydrogen in collisions with deuterium ('slow" chemistry),

$$H_2^{(1)} \;\to_{\text{wall}}\; H_2^{(0)}, \qquad H_2^{(1)} + D_2^{(0)} \;\to\; H_2^{(0)} + D_2^{(1)}.$$

The quantity to be computed is the CARS signal (coherent anti-Stokes Raman spectroscopy)

$$J(c) = \kappa \int_{-R}^{R} \sigma(s) c(r-s)^2 \,\mathrm{ds},$$

where $c(r)$ is, for example, the concentration of $D_2^{(1)}$ along the line of the laser measurement (see Segatz *et al.* [55]).

Table 6 and Figure 17 show results obtained by the DWR method for computing the mass fraction of $D_2^{(1)}$ and $D_2^{(0)}$. The comparison is against computations on heuristically refined tensor-product meshes. We observe higher accuracy on the systematically adapted meshes: particularly, monotone convergence of the desired quantities is achieved.

REMARK 4.3. More complex reactive flow problems such as combustion processes (gas-phase reactions with 'fast' chemistry) have been treated using the DWR

TABLE 6. *Results of the simulation of the relaxation experiment on heuristically adapted (left) and on automatically adapted (right) meshes (from Becker et al. [7]).*

Heuristic refinement				Adaptive refinement			
L	N	$D_2^{(\nu=0)}$	$D_2^{(\nu=1)}$	L	N	$D_2^{(\nu=0)}$	$D_2^{(\nu=1)}$
1	137	0.77613	0.00000	1	137	0.77613	0.00000
2	481	0.74222	0.00254	2	244	0.73801	0.00402
3	1793	0.78013	0.00253	3	446	0.74503	0.00260
4	1923	0.78291	0.00272	4	860	0.75665	0.00201
5	2378	0.78511	0.00171	5	1723	0.78057	0.00139
6	3380	0.79173	0.00116	6	3427	0.78588	0.00113
7	5374	0.79162	0.00143	7	7053	0.79974	0.00109

method by Braack [15]; see also Becker, Braack and Rannacher [6], and Braack and Rannacher [16].

5. Final Remarks

In this survey, we have discussed the application of duality-based methods for a posteriori error estimation and mesh adaptation for various standard types of flow problems. Limited space did not allow to consider several other new computational approaches and more involved flow situations. In the following, we list some of these developments and give hints to relevant literature.

- DG-methods for the full compressible Navier-Stokes equations for transonic and supersonic flow are described in Hartmann and Houston [34].
- Residual-based time step control in nonstationary flow computation requires the efficient computation of nonstationary dual solutions backward in time. This can be achieved by using so-called 'check-pointing' or 'windowing' techniques which are described in Becker, Meidner and Vexler [9], see also the forthcoming book Becker and Vexler [13].
- The use of residual-based mesh adaptation in computing turbulent flows is investigated in Hofmann and Johnson [39]. Here, the main claim is that turbulence modeling, for instance by small scale modeling in an LES, can be replaced by systematic residual-based mesh adaptation.
- The DWR approach for Finite Volume Methods without Galerkin orthogonality is analyzed in Giles and Pierce [25].
- Higher-order finite element methods are considered in Heuveline and Rannacher [37] for elliptic problems and in Heuveline [35] for flow problems.
- Strategies for mesh adaptation in the case of multiple target functionals, such as for example simultaneous computation of drag and lift coefficients, are proposed in Hartmann and Houston [33]).

Further important flow situations not considered in this survey are flows with free surfaces, fluid-structure interaction, flows through porous media, and micro- and capillary flows. The application of the DWR method to these kinds of flows are still to be developed.

References

1. M. Ainsworth and J. T. Oden, *A posteriori error estimation in finite element analysis*, Comput. Methods Appl. Mech. Enrg. **142** (1997), 1–88.
2. W. Bangerth and R. Rannacher, *Adaptive finite element methods for differential equations*, Birkhäuser: Basel-Boston-Berlin, 2003.
3. R. Becker, *An optimal-control approach to a posteriori error estimation for finite element discretizations of the navier-stokes equations*, East-West J. Numer. Math. **9** (2000), 257–274.
4. _____, *Mesh adaptation for stationary flow control*, J. Math. Fluid Mech. **3** (2001), 317–341.
5. R. Becker and M. Braack, *Solution of a stationary benchmark problem for natural convection with large temperature difference*, Int. J. Therm. Sci. **41** (2002), 428–439.
6. R. Becker, M. Braack, and R. Rannacher, *Numerical simulation of laminar flames at low mach number by adaptive finite elements*, Combust. Theory Modelling **3** (1999), 503–534.
7. R. Becker, M. Braack, R. Rannacher, and C. Waguet, *Fast and reliable solution of the Navier–Stokes equations including chemistry*, Comput. Visual. Sci. **2** (1999), 107–122.
8. R. Becker, V. Heuveline, and R. Rannacher, *An optimal control approach to adaptivity in computational fluid mechanics*, Int. J. Numer. Meth. Fluids. **40** (2002), 105–120.
9. R. Becker, D. Meidner, and B. Vexler, *Efficient numerical solution of parabolic optimization problems by galerkin finite element methods*, Preprint, SFB 359, Univ. of Heidelberg, 2004.
10. R. Becker and R. Rannacher, *Weighted a posteriori error control in FE methods*, Lecture at ENUMATH-95, Paris, Sept. 18-22, 1995, Preprint 96-01, SFB 359, University of Heidelberg, Proc. *ENUMATH'97* (H. G. Bock *et al.*, eds), pp. 621-637, World Scientific, Singapore, 1998.
11. _____, *A feed-back approach to error control in finite element methods: basic analysis and examples*, East-West J. Numer. Math. **4** (1996), 237–264.
12. _____, *An optimal control approach to error estimation and mesh adaptation in finite element methods*, Acta Numerica 2000 (A. Iserles, ed.), Cambridge University Press, 2001, pp. 1–101.
13. R. Becker and B. Vexler, *Optimal flow control by adaptive finite element methods*, Advances in Mathematical Fluid Mechanics, Birkhäuser, Basel-Boston-Berlin, 2005, to appear.
14. C. Bernardi, O. Bonnon, C. Langouët, and B. Métivet, *Residual error indicators for linear problems: Extension to the Navier–Stokes equations*, Proc. 9th Int. Conf. Finite Elements in Fluids, 1995.
15. M. Braack, *An adaptive finite element method for reactive flow problems*, Dissertation, Universität Heidelberg, 1998.
16. M. Braack and R. Rannacher, *Adaptive finite element methods for low-mach-number flows with chemical reactions*, 30th Computational Fluid Dynamics (H. Deconinck, ed.), Lecture Series, vol. 1999-03, von Karman Institute for Fluid Dynamics, 1999.
17. M. Braack and Th. Richter, *Solutions of 3d Navier-Stokes benchmark problems with adaptive finite elements*, submitted to Computers & Fluids, 2004.
18. S. Brenner and R. L. Scott, *The mathematical theory of finite element methods*, Springer, Berlin Heidelberg New York, 1994.
19. G. F. Carey and J. T. Oden, *Finite elements, computational aspects*, vol. III, Prentice-Hall, 1984.
20. K. Eriksson, D. Estep, P. Hansbo, and C. Johnson, *Introduction to adaptive methods for differential equations*, Acta Numerica 1995 (A. Iserles, ed.), Cambridge University Press, 1995, pp. 105–158.
21. K. Eriksson and C. Johnson, *Adaptive finite element methods for parabolic problems, I: A linear model problem*, SIAM J. Numer. Anal. **28** (1991), 43–77.
22. _____, *Adaptive finite element methods for parabolic problems, IV: Nonlinear problems*, SIAM J. Numer. Anal. **32** (1995), 1729–1749.
23. _____, *Adaptive finite element methods for parabolic problems, V: Long-time integration*, SIAM J. Numer. Anal. **32** (1995), 1750–1763.
24. M. B. Giles, M. G. Larsson, J. M. Levenstam, and E. Süli, *Adaptive error control for finite element approximations of the lift and drag coefficients in viscous flow*, Tech. report, Oxford University Computing Laboratory, 1997.
25. M. B. Giles and N. A. Pierce, *Adjoint error correction for integral outputs*, Tech. Report NA-01/18, Oxford University Computing Laboratory, 2001.

26. M. B. Giles and E. Süli, *Adjoint methods for pdes: a posteriori error analysis and postprocessing by duality*, Acta Numerica 2002 (A. Iserles, ed.), Cambridge University Press, 2002, pp. 145–236.
27. V. Girault and P. A. Raviart, *Finite element methods for Navier-Stokes equations*, Springer, Berlin-Heidelberg, 1986.
28. P. Hansbo and C. Johnson, *Adaptive streamline diffusion finite element methods for compressible flow using conservative variables*, Comput. Methods Appl. Mech. Engrg **87** (1991), 267–280.
29. R. Hartmann, *A posteriori fehlerschätzung und adaptive Schrittweiten- und Ortsgitterssteuerung bei Galerkin-Verfahren für die Wärmeleitungsgleichung*, Diploma thesis, Institute of Applied Mathematics, University of Heidelberg, 1998.
30. ———, *Adaptive finite element methgods for the compressible Euler equations*, Dissertation, Universität Heidelberg, 2002.
31. ———, *The role of the Jacobian in the adaptive discontinuous Galerkin method for the compressible Euler equations*, Analysis and Numerical Methods for Conservation Laws (G. Warnecke, ed.), Springer, 2004, to appear.
32. R. Hartmann and P. Houston, *Adaptive discontinuous Galerkin finite element methods for the compressible Euler equations*, J. Comput. Phys. **183** (2002), 508–532.
33. ———, *Goal-oriented a posteriori error estimation for multiple target functionals*, Hyperbolic problems: Theory, Numerics, Applications (T. Y. Hou and E. Tadmor, eds.), Springer, Heidelberg-New York, 2003, pp. 579–588.
34. ———, *Adaptive discontinuous Galerkin finite element methods with interior penalty for the compressible Navier-Stokes equations*, Numerical Mathematics and Advanced Applications (M. Feistauer, V. Doleji, P. Knobloch, and K. Najzar, eds.), ENUMATH 2003, Springer, 2004, pp. 410–419.
35. V. Heuveline, *On higher-order mixed FEM for low mach number flows: Application to a natural convection benchmark problem*, Internat. J. Numer. Methods Fluids **41** (2003), 1339–1356.
36. V. Heuveline and R. Rannacher, *Adaptive finite element discretization of eigenvalue problems in hydrodynamic stability theory*, Preprint, SFB 359, Universität Heidelberg, October 2004.
37. ———, *Duality-based adaptivity in the hp-finite element method*, J. Numer. Math. **11** (2003), 95–113.
38. J. Heywood, R. Rannacher, and S. Turek, *Artificial boundaries and flux and pressure conditions for the incompressible Navier-Stokes equations*, Int. J. Comput. Fluid Mech. **22** (1996), 325–352.
39. J. Hoffman and C. Johnson, *A new approach to computational turbulence modeling*, Preprint, Chalmers University of Technology, Gothenburg, `http://www.phi.chalmers.se/ preprints/`, 2004.
40. P. Houston, R. Rannacher, and E. Süli, *A posteriori error analysis for stabilized finite element approximation of transport problems*, Comput. Methods Appl. Mech. Enrg. **190** (2000), 1483–1508.
41. T. J. R. Hughes and A. N. Brooks, *Streamline upwind/Petrov Galerkin formulations for convection dominated flows with particular emphasis on the incompressible Navier–Stokes equation*, Comput. Methods Appl. Mech. Eng. **32** (1982), 199–259.
42. T. J. R. Hughes, L. P. Franca, and M. Balestra, *A new finite element formulation for computational fluid dynamics, v: Circumvent the Babuška–Brezzi condition: A stable Petrov–Galerkin formulation for the Stokes problem accommodating equal order interpolation*, Comput. Methods Appl. Mech. Enrg. **59** (1986), 89–99.
43. C. Johnson, *Numerical solution of partial differential equations by the finite element method*, Cambridge University Press, Cambridge, 1987.
44. ———, *Adaptive finite element methods for diffusion and convection problems*, Comput. Methods Appl. Mech. Eng. **82** (1990), 301–322.
45. C. Johnson, R. Rannacher, and M. Boman, *Numerics and hydrodynamic stability: Towards error control in CFD*, SIAM J. Numer. Anal. **32** (1995), 1058–1079.
46. S. Korotov, P. Neitaanmäki, and S. Repin, *A posteriori error estimation of goal-oriented quantities by the superconvergence patch recovery*, J. Numer. Math. **11** (2003), 33–53.

47. L. Machiels, A. T. Patera, and J. Peraire, *Output bound approximation for partial differential equations; application to the incompressible Navier-Stokes equations*, Industrial and Environmental Applications of Direct and Large Eddy Numerical Simulation (S. Biringen, ed.), Springer, Berlin Heidelberg New York, 1998.
48. L. Machiels, J. Peraire, and A. T. Patera, *A posteriori finite element output bounds for the incompressible Navier-Stokes equations: application to a natural convection problem*, Tech. Report 99-4, MIT FML, 1999.
49. J. T. Oden and S. Prudhomme, *On goal-oriented error estimation for elliptic problems: Application to the control of pointwise errors*, Comput. Methods Appl. Mech. Eng. **176** (1999), 313–331.
50. ———, *Estimation of modeling error in computational mechanics*, Preprint, TICAM, The University of Texas at Austin, 2002.
51. J. T. Oden, W. Wu, and M. Ainsworth, *An a posteriori error estimate for finite element approximations of the Navier–Stokes equations*, Comput. Methods Appl. Mech. Eng. **111** (1993), 185–202.
52. M. Paraschivoiu and A. T. Patera, *Hierarchical duality approach to bounds for the outputs of partial differential equations*, Comput. Methods Appl. Mech. Enrg. **158** (1998), 389–407.
53. R. Rannacher, *Finite element methods for the incompressible navier-stokes equations*, Fundamental Directions in Mathematical Fluid Mechanics (G. P. Galdi, J. Heywood, and R. Rannacher, eds.), Birkhäuser, Basel-Boston-Berlin, 2000, pp. 191–293.
54. M. Schäfer and S. Turek, *Benchmark computations of laminar flow around a cylinder (with support by f. durst, e. krause and r. rannacher)*, Flow Simulation with High-Performance Computers II (E. H. Hirschel, ed.), 1996, DFG priority research program results 1993-1995, vol. 52 of Notes Numer. Fluid Mech., Vieweg, Wiesbaden, pp. 547–566.
55. J. Segatz, R. Rannacher, J. Wichmann, C. Orlemann, T. Dreier, and J. Wolfrum, *Detailed numerical simulation in flow reactors: A new approach in measuring absolute rate constants*, J. Phys. Chem. **100** (1996), 9323–9333.
56. R. Verfürth, *A posteriori error estimates for nonlinear problems*, Numerical Methods for the Navier–Stokes Equations (F.-K. Hebeker et al., ed.), Notes Numer. Fluid Mech., vol. 47, Vieweg, Braunschweig, 1993, pp. 288–297.
57. ———, *A review of a posteriori error estimation and adaptive mesh-refinement techniques*, Wiley/Teubner, New York Stuttgart, 1996.

Institut für Angewandte Mathematik, Universität Heidelberg, Heidelberg, Germany

Current address: Institut für Angewandte Mathematik, Universität Heidelberg, 69120 Heidelberg, Germany

E-mail address: rolf.rannacher@iwr.uni-heidelberg.de